Open access • Journal Article • DOI:10.1029/96JB01923

Mantle source heterogeneity and melting processes beneath seafloor spreading centers: The East Pacific Rise, 18°–19°S — Source link

Yaoling Niu, D. Guy Waggoner, John M. Sinton, John J. Mahoney

Published on: 10 Dec 1996 - Journal of Geophysical Research (American Geophysical Union)

Topics: Incompatible element

JOURNAL OF GEOPHYSICAL RESEARCH, VOL. 101, NO. B12, PAGES 27,711–27,733, DECEMBER 10, 1996

Mantle source heterogeneity and melting processes beneath seafloor spreading centers: The East Pacific Rise, 18°-19°S

Yaoling Niu

Department of Earth Sciences, University of Queensland, Brisbane, Queensland, Australia

D. Guy Waggoner, John M. Sinton, and John J. Mahoney

Department of Geology and Geophysics, University of Hawaii, Honolulu

Abstract. We present new major and trace element and Nd-Pb-Sr isotopic data on samples from the East Pacific Rise (EPR) axis and nearby seamounts in the Hump area, 18°-19°S. Most samples studied are normal mid-ocean ridge basalt (N-MORB); four samples from the southern seamounts are enriched MORB (E-MORB). Dredge 52 samples from a southern seamount are depleted in incompatible elements yet possess "enriched" isotopic signatures. Except for the dredge 52 samples, all the samples show significant correlations between isotopic ratios and ratios of incompatible elements; that is, incompatible elements and isotopes are coupled. Sr and Nd isotopic ratios correlate significantly better with ratios of moderately incompatible elements than with ratios involving highly incompatible ones (e.g., Rb, Nb, and K) which appear to be "overenriched". Both isotopic and incompatible element ratios also correlate with the extent of melting calculated from major elements. We interpret these correlations as mixing trends resulting from melting of a heterogeneous source containing enriched ("plume-like") domains of variable sizes. Overenrichment of highly incompatible elements in E-MORB appears to be recent and is best explained by low-degree-melt infiltration in the source region prior to major melting events. The low-degree melts are primarily derived from isotopically N-MORB mantle. This low-degree melt process also explains the incompatible element-isotope decoupling throughout the EPR between 13° and 23°S. The dredge 52 samples too are consistent with such a process, but their immediate source is a site of low-degree melt generation.

Introduction

It is well known that mid-ocean ridge basalt (MORB) is dominated by incompatible-element-depleted normal tholeiite (N-MORB) [e.g., *Melson et al.*, 1976; *Basaltic Volcanism Study Project (BVSP)*, 1981]. However, less depleted and even incompatible-element-enriched basalts (E-MORB) resembling those from ocean islands are common. These observations suggest that the upper mantle beneath ocean ridges is heterogeneous. However, the origin, size, and history of the enriched heterogeneities in the dominantly N-MORB mantle remain enigmatic. Whereas E-MORB along the northern Mid-Atlantic Ridge can be ascribed to mantle plume influence [e.g., *Sun et al.*, 1975; *Schilling et al.*, 1983; *Bougault et al.*, 1988], the origin of common E-MORB along apparently plume-absent regions of the East Pacific Rise (EPR) [e.g., *Batiza et al.*, 1977; *Langmuir et al.*, 1986; *Hékinian et al.*, 1989; *Sinton et al.*, 1991; *Batiza and Niu*, 1992; *Mahoney et al.*, 1994; *Perfit et al.*, 1994; *Niu et al.*, 1994] and nearby seamounts [*Batiza and Vanko*, 1984; *Zindler et al.*, 1984; *Graham et al.*, 1988; *Batiza et al.*, 1989, 1990] is unexplained.

Large isotopic ranges in seamount rocks near the northern EPR axis [e.g., *Batiza and Vanko*, 1984; *Zindler et al.*, 1984] suggest that the size of heterogeneous mantle "domains" may be as small as a few kilometers. The correlations of radiogenic isotopes with ratios of incompatible elements [e.g., *Graham et al.*, 1988; *Niu et al.*, 1994] in lavas from the northern EPR axis and nearby seamounts indicate that the heterogeneities are ancient and may occur as "blobs" or "streaks" [e.g., *Hanson*, 1977; *Allègre et al.*, 1984; *Fitton and James*, 1986; *Saunders et al.*, 1988; *Mahoney et al.*, 1989; *Weaver*, 1991] that have survived in the convecting mantle for up to ~ 2 Gyr. In some places along the EPR axis, good correlations exist between isotopes and major element chemistry [e.g., *Castillo et al.*, 1991; *Niu et al.*, 1994], in other places, no obvious correlation is found [*Macdougall and Lugmair*, 1985, 1986; *Prinzhofer et al.*, 1989; *Mahoney et al.*, 1994], and in some places, isotopes and incompatible elements are decoupled as a result of recent mantle enrichment [*Mahoney et al.*, 1994].

In this paper, we present new major and trace element data and Nd-Pb-Sr isotopic results on lavas from the axis and nearby seamounts in the Hump area [*Cormier and Macdonald*, 1994], 18° to 19°S, on the EPR. These data provide insights into the nature of mantle source heterogeneity and melting processes.

Paper number 96JB01923.
0148-0227/96/96JB-01923$09.00

Previous Work and Regional Geology in the Hump Area

The EPR of the study area spreads asymmetrically at rates of ~45 mm/yr to the east and ~101 mm/yr to the west [*Cormier and*

Macdonald, 1994]. The approximately 1400 km^2 Hump area (Figure 1) is centered on the EPR at 18° - 19°S and is one of the best-known parts of the EPR. The rise axis and nearby flanks have been well studied by SeaMARC II and Sea Beam mapping [*Sempéré et al.*, 1987; *Lonsdale*, 1989; *Cormier and Macdonald*, 1994; *Shen et al.*, 1993], submersible observations [*Renard et al.*, 1985; *Bäcker et al.*, 1985; *Auzende et al.*, 1994], magnetics [*Perram et al.*, 1993; *Cormier and Macdonald*, 1994], seismic experiments [*Detrick et al.*, 1993], and petrological sampling and geochemical investigations [*Bäcker et al.*, 1985; *Renard et al.*, 1985; *Sinton et al.*, 1991; *Mahoney et al.*, 1994; *Bach et al.*, 1994]. The rise axis in the Hump area consists of three segments (i.e., H, I, and J of *Sinton et al.* [1991]) offset 1-3 km by two left-stepping discontinuities at 18°22'S and 18°36'S [*Lonsdale*, 1989; *Sinton et al.*, 1991], respectively, which also coincide with magmatic segment boundaries [*Sinton et al.*, 1991]. The central and northern segments have an axial summit graben (600-800 m wide and 100 m deep), with the eastern shoulder marking the shallowest part of the southern EPR axis in the vicinity. The southern segment lacks an axial summit graben and has a broad across-axis area reflecting a more robust magma supply [e.g., *Scheirer and Macdonald*, 1993]. Near-ridge seamounts on the Pacific Plate are part of a large complex of near-ridge seamount chains occurring between 15° and 19 °S [*Shen et al.*, 1993, 1995; *Sinton et al.*, 1994].

The EPR axial lavas between 13° and 23°S are dominated by N-MORB which exhibits a northward increase in incompatible element ratios (Figure 2) [*Sinton et al.*, 1991; *Mahoney et al.*, 1994]. However, E-MORB also occurs throughout the region and shows no correlations with any geological or geophysical parameters. Nd, Sr, and Pb radiogenic isotopes define a broad dome at 15.8° to 20.7°S, which correlates neither with the latitudinal trend in N-MORB incompatible element ratios nor with the occurrence of E-MORB (Figure 2). Thus incompatible elements and isotopes are decoupled along the southern EPR axis [*Mahoney et al.*, 1994]. If off-axis seamount lavas are included, the Hump area exhibits the largest chemical variation at a given latitude in the 13°-23°S region, with the most depleted and enriched lavas occurring at seamounts.

Samples, Methods, Data and Model Interpretations

The samples were dredged during cruise MW8712 of the R/V *Moana Wave*. All the samples (fresh glasses and fresh near-glass-rind portions of crystalline rocks) studied are aphyric to slightly plagioclase- and plagioclase-olivine-phyric basalts from the axis and nearby seamounts (Figure 1). Major elements and non-rare-earth trace elements were analyzed by X ray fluorescence at the University of Hawaii [see *Mahoney et al.*, 1994]. Rare earth elements were analyzed by X ray fluorescence after ion-exchange pre-concentration at the University of Tasmania [see *Robinson et al.*, 1986], and Nd-Pb-Sr isotopic ratios were analyzed at the University of Hawaii [see *Mahoney et al.*, 1994].

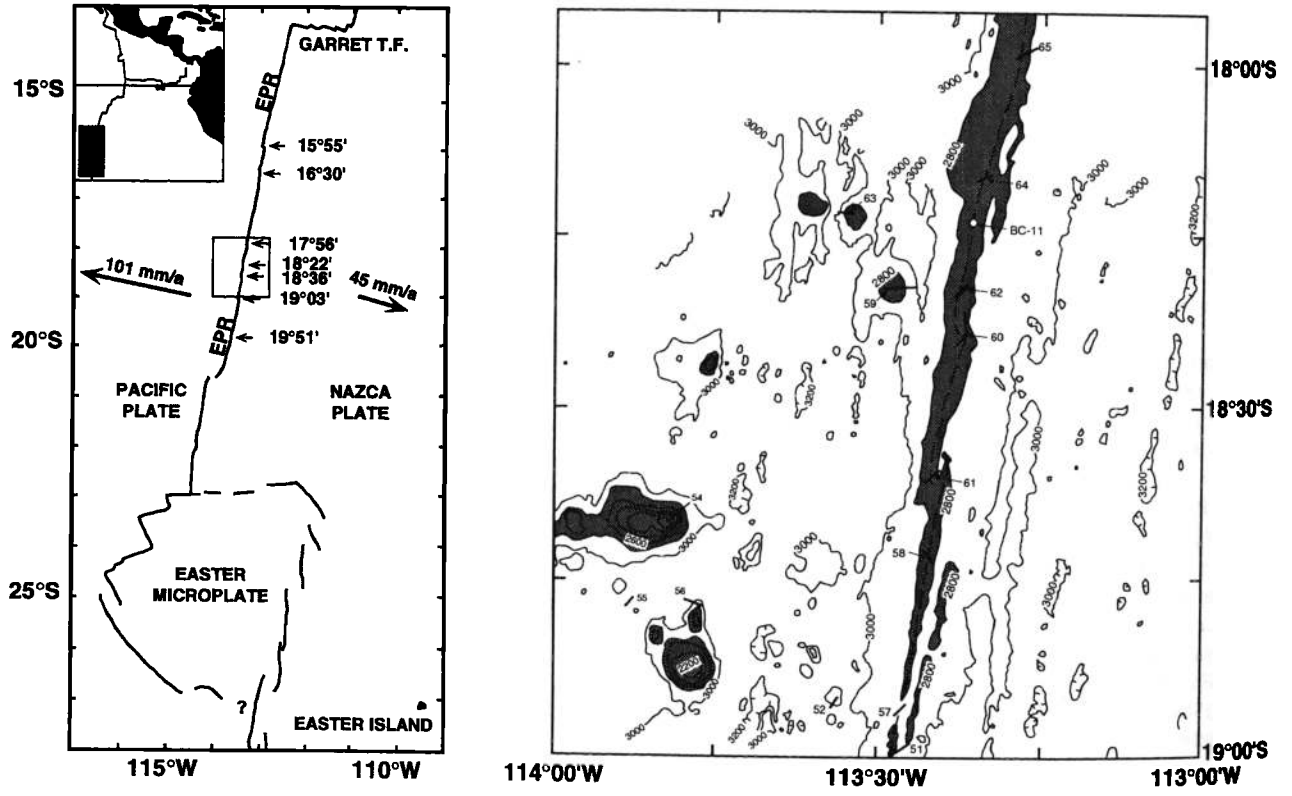

Figure 1. (left) Regional tectonic elements of the southern EPR [after *Cormier and Macdonald*, 1994], in which the Hump area is highlighted. (right) Bathymetric details of the Hump area [after *Sinton et al.*, 1991]. The stippled regions at depths less than 2800 m effectively show the rise axis and near-ridge seamounts. Numbered thick lines (51-65) are dredge tracks of Expedition MW8712 [see *Sinton et al.*, 1991]. BC-11 is the off-bottom location of bottom camera run 11 conducted during the MW8712 expedition.

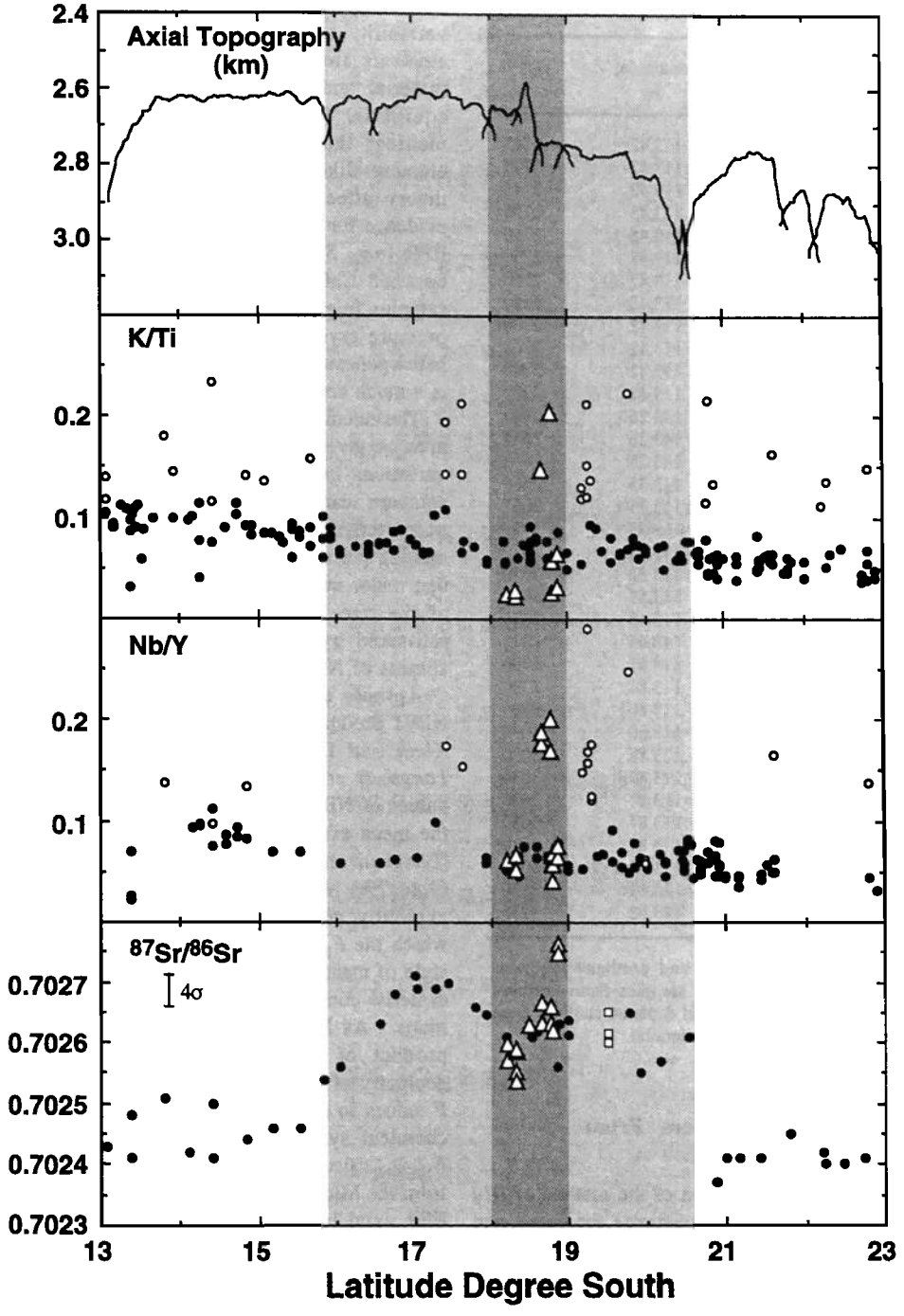

Figure 2. Previous regional studies along the southern EPR from 13° to 23°S [*Sinton et al.*, 1991; *Mahoney et al.*, 1994] showed a monotonic increase in K/Ti and Nb/Y from south to north for N-MORB samples (solid circles), with E-MORB (open circles) occurring randomly and lacking systematics. Sr isotopic ratios exhibit a broad dome between 15.8° and 20.7°S as highlighted. Open squares in the $^{87}Sr/^{86}Sr$ panel are for seamount samples of *Macdougall and Lugmair* [1985]. Note that no obvious correlations exist between isotopic ratios and ratios of incompatible elements. The darker-shaded area (18°S - 19°S) is the Hump area, with open triangles being seamount samples.

Most samples are N-MORB, except for dredges 54 and 56 samples from the southern seamount group, which are typical E-MORB (Tables 1 and 2). The samples range in MgO from 9.28 to 6.66 wt % and, in terms of mass balance, could have formed by up to 50% low-pressure fractional crystallization. Figure 3 shows that although variable fractional crystallization is important, much of the scatter at a given MgO content can only be explained by differences in parental magma compositions as the result of (1) differences in extent and depth of melting or (2) compositional variation in the source region or both. In the following sections we evaluate the relative importance of these processes.

Table 1a. Sample Locations of the Hump Area Lavas

Sample	Locations	Latitude, °S	Longitude, °W	Depth, m
58-1	H	18.72	113.42	2745
58-4	H	18.72	113.42	2745
58-5	H	18.72	113.42	2745
57-4	H	18.88	113.45	2750
57-8	H	18.88	113.45	2750
51-4	H	19.00	113.47	2750
51-5	H	19.00	113.47	2750
60-10	I	18.43	113.40	2650
61-5	I	18.60	113.42	2700
61-1	I	18.60	113.42	2700
61-3	I	18.60	113.42	2700
61-4	I	18.60	113.42	2700
65-3	J	17.94	113.26	2665
65-8	J	17.95	113.26	2665
64-2	J	18.18	113.35	2665
64-5	J	18.18	113.35	2665
64-6	J	18.18	113.35	2665
BC11-1	J	18.19	113.33	2650
62-1	J	18.35	113.38	2670
62-5	J	18.35	113.38	2670
63-2	N	18.22	113.57	3060
59-5	N	18.32	113.45	2885
59-8	N	18.32	113.45	2885
54-1	SE	18.67	113.81	2790
54-2	SE	18.67	113.81	2790
56-2	SE	18.78	113.80	3095
56-4	SE	18.78	113.80	3095
55-3	SN	18.50	113.87	3030
55-1	SN	18.80	113.87	3030
55-6	SN	18.80	113.87	3030
55-8	SN	18.80	113.87	3030
55-11	SN	18.80	113.87	3030
55-12	SN	18.80	113.87	3030
52-4	SN	18.88	113.62	3130
52-5	SN	18.88	113.62	3130

H, I, and J refer to southern, central, and northern segments following *Sinton et al.* [1991]. N refers to samples from northern seamounts. SE and SN refer to enriched and depleted samples from southern seamount (see Figure 1 and text for details).

Calculating the Melting Parameters From Major Element Data

Method. We used a modified version of the method of *Niu and Batiza* [1991a] (NB91 hereafter) to estimate the extent and pressure of melting. Application of NB91 requires that the observed MORB chemical analyses be normalized to a common MgO value of 8.0 wt % to correct for crustal-level fractionation effects [e.g., *Klein and Langmuir*, 1987]. We did so using the algorithm of *Niu* [1992]. The correction coefficients and the algorithm [e.g., *Niu*, 1992] are given in Table 3. NB91 uses Na_8 (i.e., Na_2O wt % corrected to 8.0 wt % MgO) and Ca_8/Al_8 to compute the extent of partial melting (F) and Si_8/Fe_8 to obtain the melting depth. We modified NB91 by incorporating more recent experimental data of *Hirose and Kushiro* [1993] and *Baker and Stolper* [1994] and by using Ca_8/Al_8 alone for calculating the extent of melting. Na_8 was excluded because (1) Na in the oceanic mantle may be heterogeneous [e.g., *Natland*, 1989; *Niu and Batiza*, 1994; *Shen and Forsyth*, 1995], (2) Na measurement in MORB glasses suffers large analytical uncertainties [e.g., *Nielsen et al.*, 1995], and (3) Na abundances in MORB also are affected by olivine crystallization from ascending melts in the mantle (Ca/Al ratio is unaffected; Y. Niu, manuscript in preparation, 1996).

Although Ca and Al in the mantle may not be uniform, their variability may be relatively small. This is because these elements are major (several percent) components of mantle material and their behavior is largely governed by phase equilibria, both under subsolidus conditions and during melting; this is not necessarily true for trace and minor elements like Na. Crystallization at high pressures may in theory affect CaO/Al_2O_3 ratios in the melts, but there is no evidence for high-pressure crystallization beneath the southern EPR [e.g., *Sinton et al.*, 1991]. Importantly, the correlation between CaO/Al_2O_3 and radiogenic isotopes in many MORB samples [e.g., *Niu et al.*, 1994] cannot be explained by high-pressure crystallization but is readily explained by melting a heterogeneous mantle as elaborated below. Therefore Ca_8/Al_8 is a much better parameter for estimating the extent of melting.

The calculated mean extent of melting (F_{MEAN}) for the Hump area is given in Table 4. Note that small but significant variations exist from one group to another, particularly the southern seamount group (S), which shows a much lower extent of partial melting. We have also estimated that the initial melting pressures vary between ~ 18 and ~ 23 kbar, suggesting that major melting occurs in the spinel stability field. As much of the trace element modeling in this paper uses F values estimated by NB91, it is necessary to discuss briefly the aptness of NB91.

Aptness of NB91. *Kinzler and Grove* [1993] showed that NB91 produces systematically higher F values than models of *Klein and Langmuir* [1987] and *Kinzler and Grove* [1992]. *Langmuir et al.* [1992] and *Forsyth* [1993] considered the F values of NB91 to be melting maxima (F_{MAX}) and argued that the mean extents of melting (F_{MEAN}) are one half (5 to 10%) [*Langmuir et al.*, 1992; *Kinzler and Grove*, 1993] or one third (3 to 7%) [*Forsyth*, 1993] of these values. These models explicitly consider the geometry of the melting region, in which the F_{MEAN} would be less than F_{MAX}, depending on the style of mantle upwelling. However, NB91 obtains F values by directly comparing the observed MORB melts with model melts. As MORB melts represent the pooled, averaged, net product of complex polybaric melting regardless of the geometry of the melting region and the style of upwelling, the F values so derived are thus the true F_{MEAN}. In addition, lava chemical systematics involving Ti and Na suggest that the F_{MEAN} calculated by NB91 is reasonable. As is found in lavas from the Mid-Atlantic Ridge at 26°S [*Niu and Batiza*, 1994], the EPR axial lavas [*Sinton et al.*, 1991] also show that TiO_2 is more incompatible than Na_2O during melting (Figure 4a). However, Figure 4b shows that for this to be true, the F_{MEAN} must be greater than ~16%. At F values below ~16%, Na_2O behaves more incompatibly than TiO_2, the opposite of what we see here. Although the crossover in D values (Figure 4b) may vary due to mantle source heterogeneity, the EPR MORB must be generated by > 10% melting. Our results are consistent with recent drill hole observations at Hess Deep, which indicate that melting residues beneath the EPR are harzburgitic, not lherzolitic [*Gillis et al.*, 1993].

Figure 4c, a type of diagram widely used to discriminate the initial melting depth for MORB, indicates that MORB (both N and E type) from the southern EPR axis represent melting in the spinel lherzolite depth range, not in the garnet stability depth range. Although melt contribution from greater depths [e.g., *Salters and Hart*, 1989] is possible, this contribution is insignificant beneath the southern EPR, unless (1) melting occurs primarily within the garnet stability field such that no garnet remains, or (2) significant shallow level (spinel

Table 1b. Major and Trace Element Data for the Hump Area Lavas

Sample	58-1	58-4	58-5	57-4	57-8	51-4	51-5	60-10	61-5	61-1	61-3	61-4	65-3	65-8	64-2	64-5	64-6	BC11-1
SiO_2	50.37	50.9	50.91	49.21	49.99	51.47	49.85	50.53	51.65	50.78	50.78	51.06	50.09	52.2	50.53	50.32	50.44	51.33
TiO_2	1.28	1.63	1.63	1.71	1.56	1.44	1.71	1.70	1.38	1.91	1.68	1.66	1.49	1.35	1.71	1.50	1.51	1.67
Al_2O_3	15.68	14.58	14.68	15.61	15.82	14.82	15.83	14.50	15.48	14.26	14.91	14.67	14.74	14.81	14.44	14.83	14.86	14.63
FeOt	9.28	10.58	10.60	10.38	10.03	10.17	10.26	10.85	8.93	11.78	10.66	10.66	10.66	9.50	11.40	10.51	10.59	10.84
MnO	0.17	0.19	0.19	0.19	0.18	0.20	0.19	0.20	0.18	0.21	0.19	0.19	0.20	0.19	0.20	0.19	0.19	0.20
MgO	8.56	7.33	7.38	8.00	8.15	7.45	7.71	7.11	7.27	6.66	7.27	7.24	7.64	6.90	7.08	7.56	7.59	6.66
CaO	12.17	11.80	11.86	11.50	11.64	12.05	11.58	11.63	12.41	11.15	11.57	11.78	12.00	12.06	11.56	12.05	12.04	11.85
Na_2O	2.28	2.57	2.60	2.72	2.45	2.33	2.62	2.91	2.62	2.99	2.77	2.62	2.47	2.66	2.57	2.43	2.41	2.50
K_2O	0.05	0.08	0.08	0.06	0.09	0.07	0.07	0.08	0.08	0.12	0.09	0.09	0.05	0.11	0.07	0.07	0.06	0.06
P_2O_5	0.09	0.12	0.12	0.14	0.13	0.09	0.14	0.13	0.08	0.14	0.10	0.12	0.10	0.09	0.12	0.10	0.10	0.09
Total	99.93	99.78	100.06	99.52	100.03	100.09	99.96	99.65	100.08	100.01	100.04	100.09	99.43	99.87	99.68	99.56	99.78	99.84
Mg#	64.62	57.87	57.97	60.41	61.66	59.2	59.81	56.51	61.72	52.85	57.47	57.37	58.66	58.99	55.16	58.77	58.67	54.9
Sc	43	48	46	45	44	48	44	51	49	50	47	47	49	48	51	47	48	49
V	302	359	352	322	321	354	323	356	313	389	340	361	344	335	385	349	346	383
Cr	375	158	157	340	354	223	345	131	327	50	149	137	225	136	139	240	241	145
Co	56	49	58	45	50	43	43	46	40	59	42	44	47	40	47	49	44	42
Ni	135	68	68	137	131	68	127	57	60	44	67	61	86	49	64	85	83	53
Cu	78	73	71	72	68	49	62	72	41	60	48	55	82	41	75	74	73	43
Zn	77	87	88	83	84	82	85	85	70	101	89	88	82	72	99	88	86	87
Sr	104	111	111	119	120	94	119	122	124	117	127	112	98	106	105	97	99	95
Y	30	38	38	40	35	33	39	39	30	43	35	36	36	35	41	35	36	35
Zr	77	104	102	115	101	84	114	111	97	123	111	106	86	95	104	88	89	97
Nb	2.0	2.4	2.5	3.1	2.5	1.7	2.2	2.9	2.3	2.8	2.6	2.4	2.3	2.1	2.2	2.0	1.9	2.0
La	2.66			2.96					1.97	3.87			2.50					
Ce	8.60			10.46					6.79	11.90			8.75					
Pr	1.45			1.80					1.23	2.06			1.41					
Nd	8.24			10.98					7.45	12.58			8.75					
Sm	3.12			3.68					2.67	4.44			3.54					
Eu	1.24			1.48					1.23	1.55			1.41					
Gd	4.09			5.31					4.06	5.99			4.61					
Dy	5.04			6.32					4.79	7.21			5.77					
Ho	1.08			1.41					–	1.64			–					
Er	3.35			4.26					3.11	4.82			3.82					
Yb	3.07			3.79					2.82	4.19			3.54					
$[La/Sm]_{CN}$	0.55			0.519					0.476	0.563			0.456					
$[Ce/Yb]_{CN}$	0.778			0.767					0.669	0.789			0.687					
K/Ti	0.055	0.069	0.069	0.049	0.081	0.068	0.057	0.066	0.081	0.088	0.075	0.076	0.047	0.114	0.057	0.065	0.056	0.050

Major and non-rare-earth trace elements were analyzed by X ray fluorescence at the University of Hawaii following *Mahoney et al.* [1994]. Rare earth elements were analyzed by X ray fluorescence at the University of Tasmania following *Robinson et al.* [1986]. FeOt is total iron as FeO. $Mg^{\#} = Mg/(Fe^{2+} + Mg)$ with $Fe^{2+}/(Fe^{2+} + Fe^{3+}) = 0.9$ assumed. CN is chondrite normalized.

Table 1c. Major and Trace Element Data for the Hump Area Lavas

Sample	62-1	62-5	63-2	59-5	59-8	54-1	54-2	56-2	56-4	55-3	55-1	55-6	55-8	55-11	55-12	52-4	52-5
SiO_2	50.85	50.59	50.03	49.91	50.65	48.98	49.11	48.63	48.58	48.83	48.74	48.84	49.82	48.75	48.64	48.44	48.78
TiO_2	1.60	1.46	1.15	0.95	1.33	1.68	1.72	1.64	1.97	1.73	1.73	1.73	1.39	1.75	1.72	1.66	1.65
Al_2O_3	14.53	15.01	15.25	15.19	14.34	17.09	17.09	16.18	15.97	16.22	16.20	16.20	17.83	16.11	16.02	15.55	15.53
FeOt	10.84	9.72	9.24	9.15	11.13	9.84	8.99	9.92	9.99	9.64	9.62	9.64	7.68	9.76	9.67	10.86	10.77
MnO	0.19	0.17	0.17	0.17	0.20	0.16	0.16	0.16	0.18	0.17	0.18	0.17	0.14	0.18	0.18	0.19	0.19
MgO	7.30	7.68	8.41	9.06	7.57	7.63	7.56	9.05	8.58	9.26	9.21	9.28	7.98	9.22	9.16	8.89	8.77
CaO	11.86	12.27	12.81	13.07	12.09	11.22	11.26	10.67	10.35	11.01	11.02	11.03	11.93	11.02	11.00	10.89	11.07
Na_2O	2.55	2.47	2.20	1.74	2.28	2.93	3.20	2.90	3.42	2.88	2.87	2.86	2.72	2.89	2.82	2.87	2.85
K_2O	0.10	0.09	0.01	0.02	0.02	0.34	0.37	0.26	0.27	0.08	0.06	0.06	0.03	0.07	0.06	0.06	0.06
P_2O_5	0.09	0.09	0.07	0.05	0.07	0.20	0.19	0.20	0.24	0.12	0.13	0.12	0.07	0.13	0.13	0.11	0.11
Total	99.91	99.55	99.43	99.31	99.68	100.07	99.65	99.61	99.56	99.94	99.76	99.93	99.59	99.87	99.39	99.54	99.79
$Mg^{\#}$	57.13	61.01	64.32	66.25	57.4	60.56	62.51	64.37	62.99	65.54	65.46	65.59	67.27	65.17	65.23	61.86	61.73
Sc	45	46	46	44	48	35	36	34	38	40	42	40	40	40	41	45	44
V	356	320	296	291	360	255	264	260	285	278	276	265	236	274	278	300	294
Cr	180	353	434	423	104	263	259	384	343	433	437	412	557	404	432	360	356
Co	44	41	49	50	52	43	44	48	50	71	50	48	74	64	67	51	53
Ni	65	79	97	106	47	138	131	207	199	217	217	214	206	215	212	205	194
Cu	57	58	86	92	80	67	68	64	64	72	70	69	51	71	70	79	79
Zn	90	79	69	68	87	73	70	77	86	80	77	78	56	78	79	84	84
Sr	101	108	80	55	60	204	201	178	171	159	159	161	174	158	159	129	128
Y	36	32	28	25	34	33	34	34	43	37	38	38	28	38	38	38	38
Zr	93	88	59	40	60	136	136	133	167	127	126	127	102	129	127	105	104
Nb	1.7	2.1	1.7	1.7	1.8	5.9	6.4	6.7	7.3	2.5	2.1	2.6	1.1	2.6	2.2	2.4	2.9
La			1.39	1.17		4.92	5.95		6.99		3.8		2.81			2.58	
Ce			4.60	3.87		14.82	17.20		21.07		13.57		9.00			9.75	
Pr			0.80	0.69		2.41	2.58		3.21		2.23		1.52			1.57	
Nd			5.86	4.93		12.94	13.82		16.90		12.94		9.43			9.55	
Sm			2.61	2.13		4.00	4.58		5.24		4.24		3.78			3.46	
Eu			1.09	0.84		1.37	1.76		1.81		1.50		1.46			1.23	
Gd			3.95	3.09		5.13	5.47		6.28		5.31		5.08			4.91	
Dy			4.59	4.06		5.58	6.13		7.29		6.36		–			5.91	
Ho			1.00	–		–	1.28		1.45		1.30		–			–	
Er			3.02	2.73		–	3.87		4.62		3.85		4.08			3.99	
Yb			2.95	2.42		3.27	3.35		4.02		3.49		4.23			3.89	
$[La/Sm]_{CN}$			0.344	0.355		0.794	0.839		0.861		0.579		0.480			0.481	
$[Ce/Yb]_{CN}$			0.433	0.444		1.259	1.426		1.456		1.080		0.591			0.696	
K/Ti	0.088	0.087	0.121	0.029	0.021	0.280	0.301	0.220	0.192	0.065	0.049	0.049	0.030	0.056	0.049	0.051	0.051

Major and non-rare-earth trace elements were analyzed by X ray fluorescence at the University of Hawaii following *Mahoney et al.* [1994]. Rare earth elements were analyzed by X ray fluorescence at the University of Tasmania following *Robinson et al.* [1986]. FeOt is total iron as FeO. $Mg^{\#} = Mg/(Fe^{2+} + Mg)$ with $Fe^{2+}/(Fe^{2+} + Fe^{3+}) = 0.9$ assumed. CN is chondrite normalized.

Table 2. Radiogenic Isotope and Isotope-Dilution Trace Element Data for the Hump Area Lavas

Sample	$^{206}Pb/^{204}Pb$	$^{207}Pb/^{204}Pb$	$^{208}Pb/^{204}Pb$	$^{87}Sr/^{86}Sr$	$^{143}Nd/^{144}Nd$	ε_{Nd}	Pb	Rb	Sr	Sm	Nd
					Northern Seamounts						
59-3	18.445	15.484	37.909	0.70255	0.513173	10.4	0.179	0.15	59.1	2.622	6.136
59-4	18.491	15.497	37.949	0.70259	0.513136	9.7	0.127	0.10	55.2	1.860	4.283
59-5	18.488	15.498	37.955	0.70259	0.513141	9.8	0.131	0.11	55.5	1.901	4.392
59-8	18.454	15.496	37.942	0.70254	0.513144	9.8	0.197	0.09	58.0	2.594	6.058
63-1	18.487	15.486	37.939	0.70257	0.513141	9.8	0.216	0.18	81.5	2.406	6.126
63-2	18.491	15.494	37.979	0.70260	0.513141	9.8	0.232	0.19	81.6	2.406	6.130
					Southern Seamounts						
52-4	18.805	15.528	38.335	0.70276	0.513070	8.4	0.375	0.37	134.1	3.461	9.797
52-5	18.797	15.524	38.308	0.70275	0.513086	8.7	0.439	0.36	133.1	3.433	9.717
54-1	18.758	15.530	38.310	0.70263	0.513096	8.9	0.590	2.63	202.8	4.000	13.08
54-2	18.735	15.524	38.290	0.70266	0.513109	9.1	0.617	2.54	197.5	3.916	12.82
54-3	18.760	15.529	38.318	0.70267	0.513114	9.2	0.741	2.63	201.7	4.039	13.19
55-3	18.518	15.499	38.004	0.70263	0.513091	8.8	0.512	0.42	166.7	3.970	11.86
55-8	18.513	15.491	37.947	0.70026	0.513116	9.3	0.426	0.10	158.7	2.727	8.039
56-2	18.828	15.527	38.398	0.70266	0.513100	9.0	0.695	3.30	176.6	3.914	12.87
56-4	18.620	15.521	38.152	0.70263	0.513107	9.1	0.665	2.23	166.9	4.721	15.18
					Hump axial						
51-4	18.561	15.508	38.123	0.70264	0.513122	9.4	0.315	0.41	97.0	3.175	8.493
51-5	18.559	15.507	38.075	0.70261	0.513118	9.3	0.390	0.40	97.3	3.186	8.520
57-4	18.514	15.490	38.017	0.70026	0.513115	9.3	0.401	0.48	114.7	3.581	10.17
61-1	18.516	15.498	38.053	0.70262	0.513121	9.4	0.488	0.56	122.7	4.408	12.43
BC-11	18.567	15.515	38.085	0.70261	0.513114	9.2	0.346	0.39	98.3	3.642	9.724
65-3	18.550	15.507	38.051	0.70265	0.513122	9.4	0.300	0.46	96.4	3.064	8.192

Pb isotopic ratios are corrected for fractionation relative to the National Institute of Standards and Technology NBS 981 values of *Todt et al.* [1984]. Nd isotopes were analyzed as oxides, and the isotopic fractionation correction applied was $^{148}NdO/^{144}NdO = 0.242436$ ($^{148}Nd/^{144}Nd = 0.241572$). The fractionation correction used for Sr was $^{87}Sr/^{86}Sr = 0.1194$. Nd isotopic data are reported relative to the measured $^{143}Nd/^{144}Nd$ values for the La Jolla Nd standard of 0.511855 ± 0.000012 total range. Sr isotopic data are reported relative to a $^{87}Sr/^{86}Sr$ value of 0.71025 for NBS 987. The measured $^{87}Sr/^{86}Sr$ for NBS 987 during the tenure of this study was 0.71025 ± 0.00002 total range. Variations on $^{206}Pb/^{204}Pb$ are less than ±0.012, on $^{207}Pb/^{204}Pb$ less than ±0.012, and on $^{208}Pb/^{204}Pb$ less than ±0.038. Within-run uncertainties on Pb, Sr, and Nd isotopic ratios are less than the total ranges measured on NBS 981, NBS 987, and the Lo Jolla. Total procedural blanks are < 40 pg for Pb, < 20 pg for Nd, < 120 pg for Sr; all blanks are negligible for these analyses. Trace element concentrations are in parts per million.

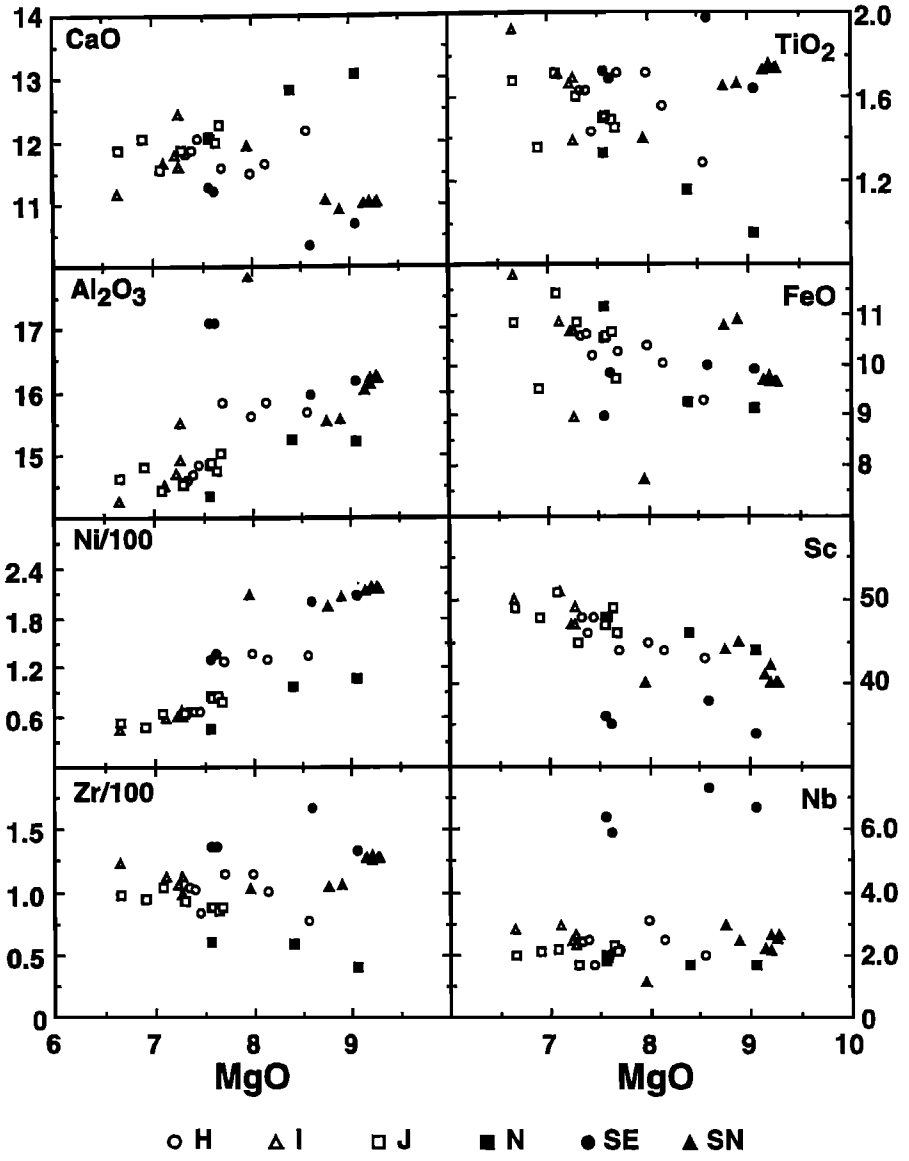

Figure 3. MgO variation diagrams of representative major, minor, and trace elements of the Hump area lavas. H, I, and J are magmatic segments of *Sinton et al.* [1991]. N represents northern seamount lavas, and SE and SN represent enriched and depleted lavas from the southern seamounts, respectively. Total iron is as FeO.

lherzolite depth range) melt-solid equilibration eradicates high-pressure signatures. These two scenarios are possible, but further evidence is required. We emphasize that our calculated melting depth range is consistent with major and trace element data.

Effects of Melting Conditions on Lava Chemical Diversity

Extent of melting versus trace element and isotope systematics. *Mahoney et al.* [1994] showed that along the southern EPR axis (13° to 23°S), radiogenic isotopes correlate neither with incompatible element ratios nor with melting parameters inferred from major elements, primarily because of the comparatively small range in chemical compositions of the axial lavas. The new data from the Hump area seamount lavas exhibit several-fold larger variations than the axial lavas and show significant (at > 99% confidence levels) correlations among radiogenic isotopes, ratios of incompatible elements, and the extent of melting estimated from major elements (Figures 5 - 7). Given the relative bulk distribution coefficients (D) of each elemental pair in Figure 5, these correlations are expected as a result of varying extents of melting. However, the correlations are significantly better for ratios of moderately/slightly incompatible elements than for those involving highly incompatible elements (e.g., Rb, Nb, and K). The excessively elevated ratios involving highly incompatible elements for lavas with low extents of melting (southern seamount E-MORB), although qualitatively consistent with melting, cannot be explained by melting of a uniform source. In particular, the significant correlations between isotopic ratios and the extent of melting (Figure 6) suggest that the mantle source for the Hump area lavas is heterogeneous, yet the observed systematics of the heterogeneity is related to melting processes (see below).

Table 3. Coefficients Used to Correct the Observed Oxides to MgO = 8.0

	m_1	m_2	m_3	m_4
SiO_2	-9.5261	1.2242	-0.0532	0
TiO_2	6.9928	-1.5294	0.1305	-0.0039
Al_2O_3	-3.7912	0.6477	-0.0297	1.5876e-5
FeO	14.8703	-2.9130	0.2100	-0.0049
CaO	0.7951	0.1405	-0.0127	0
Na_2O	-0.8958	0.0796	-0.0029	0
K_2O	-0.1817	0.0091	0	0
P_2O_5	-0.0940	0.0050	0	0

The coefficients are obtained based on J. M. Sinton's unpublished data (1996) of 140 southern EPR samples. Oxides at MgO = 8.0 wt % were calculated following *Niu* [1992], who used the general equation $Oxide_{(8.0)} = Oxide_{(data)} + \Sigma m_n(8^n - MgO^n)$, where $Oxide_{(data)}$ and $Oxide_{(8.0)}$ are observed values of a non-MgO oxide and that corrected to MgO = 8.0 wt%, respectively. Here n is the order of regression, and m_n is the corresponding regression coefficients. The validity of the coefficients so determined is tested by showing (1) $\Sigma Oxide_{(8.0)} + 8 = 100\pm1\%$ and (2) $Oxide_{(8.0)} \neq f(MgO)$.

The $^{87}Sr/^{86}Sr$ and $^{143}Nd/^{144}Nd$ also correlate better with ratios of less incompatible elements (e.g., Sm/Nd) than with ratios involving a highly incompatible element (e.g., Rb/Sr) (Figure 7). Pb isotopes show significant correlations with both ratios, but the correlations are better for Rb/Sr than for Sm/Nd. This correlation may reflect the well-separated bimodal Pb isotope ratios, which show high values for southern seamount E-MORB and low values for the rest of the samples, as is apparent in Figure 6.

Melting-induced mixing and pseudoisochrons. The most important implication of Figure 7 is that these correlations represent, to a first order, binary mixing (excluding the two dredge 52 samples) between an enriched component (e.g., the southern seamount E-MORB) with more radiogenic Sr and Pb and less radiogenic Nd and a depleted end-member (e.g., the northern seamount N-MORB). Indeed, melting itself is an efficient mixing process if (1) mantle in the melting region is heterogeneous and (2) the size of the enriched "domains" is small and their distribution is not uniform. The scatter about the regression lines (see Figure 7) may partly

Table 4. Model Extent of Melting, Primary Melt Composition ($Mg^{\#}$), and Extent of Crustal-Level Fractionation of the Hump Area Lavas

Sample	Location	F (%)	$Mg^{\#}$ (Primary)	$Mg^{\#}$ (data)	FLR	Pl	Ol	Cpx	f.Pl	f.Ol	f.Cpx
58-1	H	19.04	72.16	64.62	0.747	0.123	0.130	–	0.486	0.514	–
58-4	H	19.09	72.59	57.87	0.564	0.240	0.171	0.026	0.550	0.391	0.059
58-5	H	18.86	72.49	57.97	0.562	0.242	0.172	0.025	0.552	0.392	0.056
57-4	H	16.57	71.56	60.41	0.638	0.207	0.155	–	0.571	0.429	–
57-8	H	17.84	71.86	61.66	0.678	0.175	0.147	–	0.543	0.457	–
51-4	H	20.29	72.93	59.20	0.593	0.216	0.166	0.025	0.531	0.407	0.062
51-5	H	17.28	72.10	59.81	0.612	0.227	0.161	–	0.585	0.415	–
60-10	I	17.44	72.52	56.51	0.515	0.282	0.172	0.031	0.582	0.356	0.063
61-5	I	18.81	74.73	61.72	0.529	0.294	0.148	0.030	0.624	0.313	0.063
61-1	I	17.35	72.45	52.85	0.452	0.312	0.180	0.056	0.568	0.329	0.103
61-3	I	17.62	72.49	57.47	0.550	0.262	0.169	0.018	0.583	0.376	0.041
61-4	I	18.83	72.65	57.37	0.547	0.252	0.170	0.031	0.556	0.376	0.068
65-3	K	19.38	72.07	58.66	0.632	0.192	0.171	0.005	0.522	0.464	0.014
65-8	K	19.21	74.96	58.99	0.477	0.317	0.152	0.054	0.607	0.290	0.104
64-2	K	19.23	72.24	55.16	0.510	0.258	0.182	0.051	0.526	0.371	0.103
64-5	K	19.64	72.30	58.77	0.615	0.202	0.170	0.013	0.526	0.441	0.034
64-6	K	19.69	72.24	58.67	0.612	0.202	0.170	0.016	0.521	0.439	0.040
BC11-1	K	20.28	73.60	54.90	0.448	0.297	0.174	0.081	0.538	0.316	0.146
62-1	K	19.34	72.43	57.13	0.556	0.238	0.174	0.033	0.535	0.391	0.074
62-5	K	19.41	72.82	61.01	0.616	0.215	0.162	0.008	0.559	0.421	0.020
63-2	N	20.57	72.38	64.32	0.747	0.114	0.139	–	0.450	0.550	–
59-5	N	22.95	72.11	66.25	0.882	–	0.118	–	–	1.000	–
59-8	N	20.87	72.02	57.40	0.618	0.180	0.177	0.025	0.471	0.463	0.066
54-1	SE	14.61	72.16	60.56	0.568	0.279	0.153	–	0.646	0.354	–
54-2	SE	13.32	73.28	62.51	0.541	0.320	0.139	–	0.697	0.303	–
56-2	SE	13.63	72.16	64.37	0.758	0.138	0.104	–	0.571	0.429	–
56-4	SE	11.10	70.78	62.99	0.649	0.232	0.119	–	0.660	0.340	–
55-3	SN	13.92	70.85	65.54	0.795	0.112	0.093	–	0.546	0.454	–
55-1	SN	14.04	70.89	65.46	0.797	0.110	0.093	–	0.543	0.457	–
55-6	SN	14.05	70.85	65.59	0.815	0.097	0.089	–	0.523	0.477	–
55-8	SN	15.53	74.54	67.27	0.593	0.285	0.122	–	0.700	0.300	–
55-11	SN	13.98	70.80	65.17	0.796	0.110	0.094	–	0.538	0.462	–
55-12	SN	14.42	70.91	65.23	0.786	0.115	0.099	–	0.536	0.464	–
52-4	SN	14.53	70.43	61.86	0.752	0.129	0.119	–	0.521	0.479	–
52-5	SN	14.92	70.61	61.73	0.744	0.134	0.122	–	0.525	0.475	–

F is the estimated extent of melting using *Niu and Batiza* [1991a]. $Mg^{\#}$ (primary) represents the calculated primary polybaric melts. FLR is the fraction of liquid remaining after fractional crystallization from the primary melts to the observed compositions. Pl, Ol, and Cpx are plagioclase, olivine, and clinopyroxene fractions crystallized from the primary melts, calculated using the liquid line of descent model of *Weaver and Langmuir* [1990]. Here f.Pl, f.Ol, and f.Cpx are the mean fractions of these phases crystallized and are used to calculate the bulk D necessary to calculate trace element abundances in the primary melts.

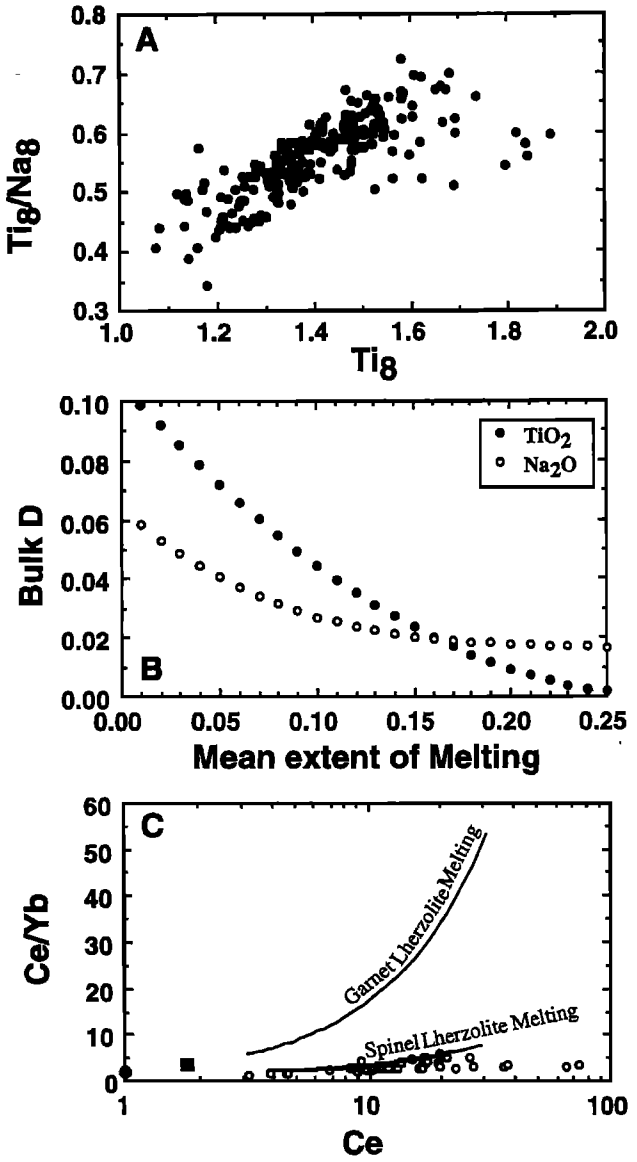

Figure 4. (a) Ti_8/Na_8 versus Ti_8 diagram [*Niu and Batiza*, 1994] for the 13° - 23°S EPR lavas [*Sinton et al.*, 1991], showing that Ti is more incompatible than Na. (b) Bulk distribution coefficient (D) for both Na_2O and TiO_2 versus mean extent of melting during peridotite melting. The D values are from *Niu and Batiza* [1991a] and *Baker and Stolper* [1994]. Na_2O is more incompatible than TiO_2 at $F_{MEAN} < \sim 16\%$, but at $F_{MEAN} > 15\%$, the opposite is true, suggesting that lavas from the southern EPR represent $F_{MEAN} > 16\%$. (c) Ce/Yb versus Ce (J. M. Sinton unpublished data, 1996) showing that the southern EPR axial lavas define a trend that is readily explained by melting in the spinel lherzolite depth range. The large solid circle is the model Hump mean source (HMS), and the large solid square is the primitive mantle of *Sun and McDonough* [1989]. Melting paths represent 0.5-25% melting in spinel lherzolite and 0.5-20% melting in garnet lherzolite calculated as in Figures 8-9 (see below). The extended range of the data beyond the ends of the spinel lherzolite melting curve indicates variations in mantle source and the effect of fractional crystallization.

reflect the nonuniform distribution of the enriched heterogeneities in the melting mantle or intrinsic heterogeneities in the enriched domains and/or the ambient depleted mantle.

From Figure 7, we obtained Rb-Sr and Sm-Nd pseudoisochron ages of 219 ± 122 Ma and 107 ± 20 Ma, respectively. Clearly, the Rb-Sr "age" is insignificant given the very large uncertainty due to Rb "overenrichment" and the effect of variable amounts of plagioclase fractionation on Sr abundances, but the age value of the Sm-Nd pseudoisochron is statistically significant. Sm-Nd "isochron" ages have been reported at several other locations along the EPR axis and from near-ridge seamounts [*Zindler et al.*, 1984; *Niu et al.*, 1994]. *Zindler et al.* [1984] suggested that they may have some time significance. Given that (1) the slopes of the isochrons are entirely defined by the positions of the two end-members in $^{143}Nd/^{144}Nd$ versus Sm/Nd space and (2) the two end-members are unlikely to have ever been "comagmatic", we consider these mixing-type isochrons unlikely to be of chronological significance. The statistically significant correlations would only imply that both the enriched component and the ambient depleted mantle are fairly ancient and have independently developed their distinct chemical and isotopic signatures.

Incompatible Trace Element Systematics in the Mantle Source

In order to fully reveal the origin of mantle source heterogeneity and to ultimately understand mantle melting processes, it is necessary to know the chemical systematics of incompatible trace elements in the source prior to the major melting events. For this purpose, we conducted a simple, two-step, inverse modeling exercise: (1) correction for the effects of fractional crystallization and (2) correction for the effects of melting. The technique is explicit, requiring no interpretation in contrast to more complicated models [e.g., *McKenzie and O'Nions*, 1991]. We first determined trace element abundances in the primary melts, which are then used to calculate their abundances in the source.

Trace element systematics in the primary melts. Assuming a uniform (major elements) mantle of the type proposed by *Hart and Zindler* [1986] (accurate knowledge of mantle composition is unimportant for the purpose) and using the calculated melting parameters and algorithms of NB91[see *Niu and Batiza*, 1991a], we obtained a parental magma composition corresponding to each sample studied. Table 4 gives the $Mg^{\#}$ of these calculated primary melts together with the observed $Mg^{\#}$. Assuming that cooling and crystallization primarily occur at crustal levels [e.g., *O'Hara*, 1968; *Walker et al.*, 1979; *Sinton and Detrick*, 1992], we obtained the overall extent of fractional crystallization and the amount of each mineral phase crystallized (Table 4) using the liquid line of descent algorithm of *Weaver and Langmuir* [1990]. We then acquired the trace element abundances in the primary magmas using these results in combination with the well-known Rayleigh fractionation algorithm and the trace element partition coefficients (Table 5).

Figure 8 shows incompatible element variations in the calculated primary magmas. We also show melting paths in both spinel and garnet lherzolite depth ranges from an assumed uniform source, which we term Hump mean source (HMS). Note that except for the enriched lavas from the southern seamount group (SE), all the data points define trends that are consistent with varying extents of melting in the spinel lherzolite depth range. However, the corresponding F values vary from ~ 5% to ~ 25% (varying from plot to plot), much greater than obtained from the major elements (Table 4). The large range of F values (Figure 8) emphasizes that the assumption of a uniform mantle

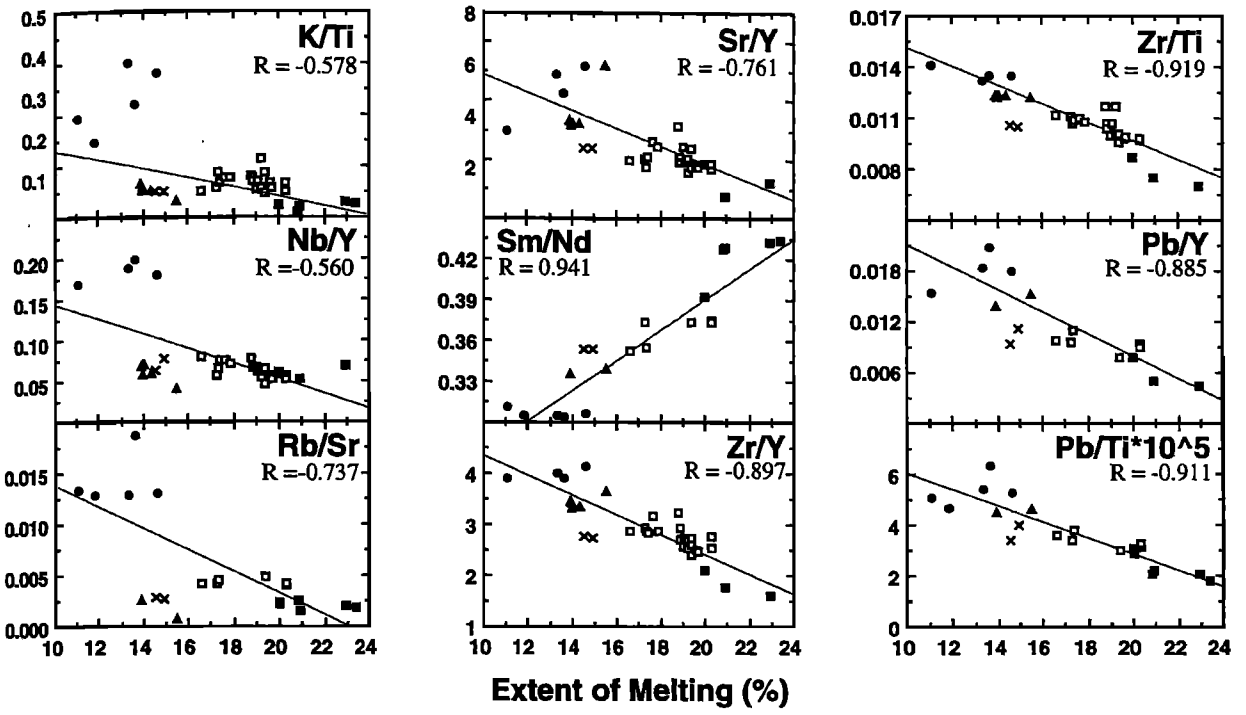

Figure 5. Incompatible trace element ratios versus the extent of melting derived from major elements. Symbols are as in Figure 3 except that all axial samples are open squares and two samples (dredge 52, crosses) from a southern seamount near the axis are highlighted because of their distinctive isotopic signatures. Note that the correlations are significantly better for ratios of moderately/slightly incompatible elements than those involving highly incompatible ones (e.g., Rb, Nb, and K).

source is invalid for incompatible elements. Also, it is clear that the SE lavas are overenriched in incompatible elements and more enriched in highly incompatible elements (e.g., Nb and K) than in moderately to slightly incompatible ones, although, isotopically, the SE lavas represent the enriched component required for the melting-induced mixing (Figure 8). This indicates that the SE lavas reflect a source that has undergone additional incompatible element enrichment. In addition, the deviation of the SE group lavas from the spinel lherzolite melting path on some plots may be interpreted as melt mixing with significant melt contribution from garnet lherzolite. This is, however, not the case (see below).

A series of ratio-element variation diagrams magnifies the inconsistencies of the estimated extent of melting one would get from one plot to another if a uniform source were assumed (Figure 9; the total range now is from 3% to >> 25%). Note that on the Ce/Yb versus Ce diagram, all the lavas, including the SE group, define a tight trend consistent with melting in the spinel lherzolite depth range. Comparing this with the Ce versus Yb plot (Figure 8), it is obvious that the SE group must be derived from spinel lherzolite, yet the elevated Ce values reflect "overenrichment" (relative to Yb). In other words, Yb is not depleted enough for significant melting at a greater depth where garnet is a residual phase.

Trace element systematics in the mantle source region. Assuming that the extent of melting calculated from major elements is correct and that the incompatible trace elements are derived from the same parcel of mantle as the major elements, then the trace element abundances of the mantle source region can be calculated using the primary magma compositions, the extent of melting determined from major elements, relevant partition coefficients (Table 5), and the information on melting modes (see caption to Figure 8). In the calculations, we assume that melting for the Hump area lavas initiates primarily in the spinel lherzolite depth range. We also assume fractional melting.

Figure 10 shows the same set of ratio-element diagrams as in Figure 9 for the calculated Hump mantle-source abundances. These plots exhibit several features: (1) the mantle source beneath the Hump area is compositionally heterogeneous with respect to the trace elements studied; (2) except for the SE group, all the data points define trends that are consistent with various extents of previous melt depletion; (3) the trends converge, more or less, toward the primitive mantle composition of *Sun and McDonough* [1989] (PM-SM); and (4) in the plots where the two melting paths (from garnet and spinel lherzolite sources, respectively) are well separated (i.e., P/Ti versus P, Y/P versus P, Y/Sr versus Sr, and Ce/Yb versus Ce), it seems that the previous melt depletion may have occurred in the garnet stability field. Assuming that the PM-SM, indeed, represents the original fertile mantle and is compositionally uniform, then the Hump source variation represents 1-3% melt removal (excepting the SE group) prior to the major melting episode that generated the lavas of the Hump area. The SE group, characterized by its closeness to PM-SM and deviation from the depletion/melting trend of the other data, indicates an additional enrichment, because the SE group is enriched in every incompatible element and the extent of enrichment is systematically greater for more incompatible elements than for less incompatible ones.

Discussion

A Cautionary Note on Trace Element Modeling

It is well known that mantle sources beneath ocean ridges can be quite heterogeneous with respect to incompatible trace

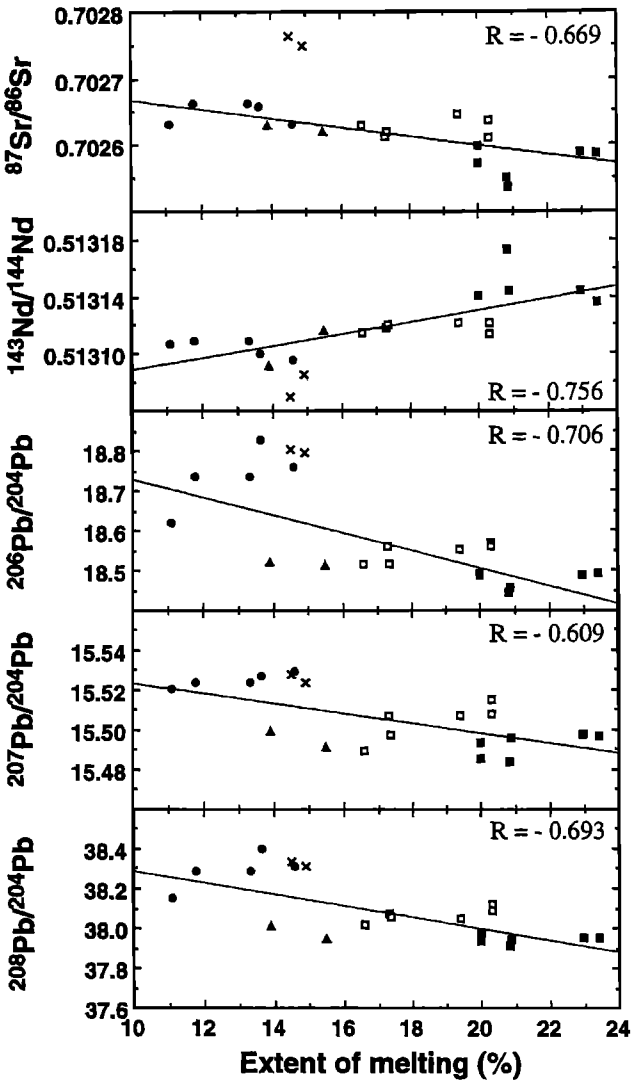

Figure 6. Radiogenic isotopic ratios versus the extent of melting derived from major elements. Symbols are as in Figure 5. The correlation coefficients, excluding the two dredge 52 samples (crosses), are significant at a > 95% confidence level.

elements on various scales. However, using variations of incompatible trace elements in MORB to model mantle melting processes remains popular. We emphasize that using trace elements alone will lead to misleading results. For example, incompatible trace element abundances in the Hump area lavas vary considerably (Figures 8 and 9). If one uses these variations to estimate the extent of melting, a very large range of F values is obtained, and these values also vary depending upon the elements and the type of diagrams used. Clearly, such large incompatible trace element variations in the Hump area lavas result largely from variations in the source region (Figure 10). So-called dynamic melting [e.g., *Langmuir et al.*, 1977; *Wood*, 1979] and other complicated perceptions of melting [e.g., *Perfit et al.*, 1983; *Clague et al.*, 1981] invoked to explain "unexpected" incompatible element variations are inappropriate here as they use single uniform source composition to model partial melting.

We stress again that major element (e.g., Si, Al, Fe, Ca, etc.) data preserve primary information on the melting processes, as they are the principal mantle mineral constituents, and their behavior is governed largely by stoichiometry and phase equilibria both under subsolidus conditions and during melting, which are intrinsically constrained by the physical conditions in the mantle [e.g., *Hanson and Langmuir*, 1978]. Incompatible trace elements, on the other hand, preserve primary information on mantle source characteristics inherited from mantle processes in the past.

Consequence of Melting a Heterogeneous Mantle Source

The chemical diversity of the Hump area lavas reflects both source heterogeneity and variable extents of melting as manifested by the significant correlations of incompatible element ratios and isotopic ratios (Figures 5 and 6) with the extent of melting derived from major elements. Incompatible-element-enriched heterogeneities are also enriched in volatiles (e.g., H_2O and CO_2, etc.) [*Aggrey et al.*, 1988; *Michael*, 1995; *Kingsley and Schilling*, 1995]; they thus should have lower melting points [e.g., *Kushiro et al.*, 1968; *Mysen and Boettcher*, 1975; *Stolper and Newman*, 1994], and their proportions in the melt decrease with further melting as a result of dilution (see Figures 5 and 6). These correlations indicate that the enriched heterogeneities represent small, yet recognizable, "domains" that are dispersed nonuniformly in the ambient depleted mantle prior to major melting events. In this regard, the correlations in Figures 5 and 7 simply represent mixing between depleted mantle and enriched heterogeneities, with the mixing being accomplished through variable amounts of melting. In summary, the geochemical consequence of melting a heterogeneous source is to produce mixing relationships in the melts between the depleted mantle end-member and an enriched component, primarily achieved through processes of melting and melt aggregation. The mixing relationships thus provide limits on the size and distribution of the enriched "domains" in the ambient depleted mantle.

N-MORB Mantle Source Heterogeneity Beneath the Hump Area

The N-MORB mantle source heterogeneity can be explained as indicating a previous depletion due to melting (Figure 10). There is a suggestion (e.g., P/Ti versus P, Y/P versus P, Sr/Y versus Sr, and Ce/Yb versus Ce) that the previous melt depletion may have taken place at depths where garnet is a residual phase. If the depleted MORB mantle on a global scale is similar in trace element abundances to those in Figure 10 and reflects 1% to 3% melt removal from the PM-SM, then the implication is important. It is widely believed that N-MORB mantle was created as the result of continental crust extraction early in the Earth's history by a few percent melting of primitive mantle [e.g., *Hofmann*, 1988; *O'Nions and McKenzie*, 1988; *Stolper and Newman*, 1994]. However, more rigorous investigations using data with a global coverage are required to examine whether such a process can explain the N-MORB mantle heterogeneity on a scale as small as the Hump area.

On the primitive-mantle-normalized diagram (Figure 11), the Hump area N-MORB source patterns can be explained by such low-degree (1-3%) melt removal, particularly for elements less incompatible than Pb. For highly incompatible elements (e.g., Rb, Nb, and K), the estimated source abundances are less depleted than expected due to melting, reflecting some recent

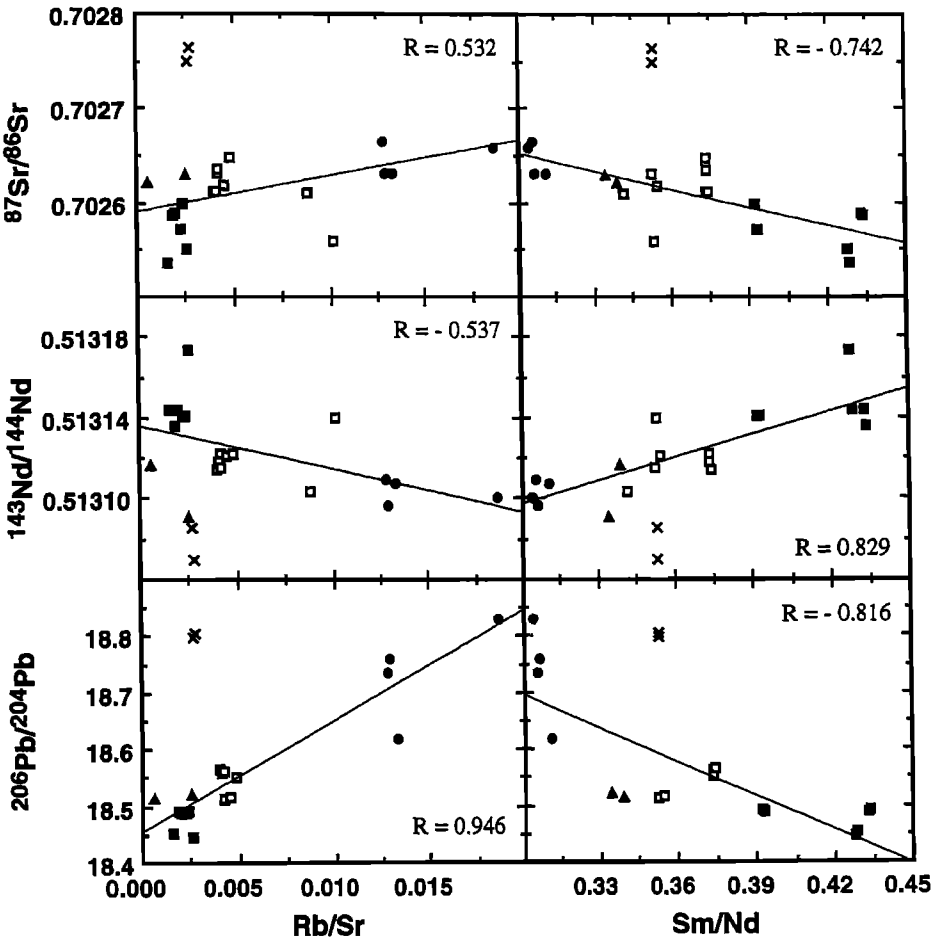

Figure 7. Covariations of isotopic ratios with ratios involving highly incompatible trace elements (e.g., Rb in Rb/Sr) and ratios of moderately/slightly incompatible ones (Sm/Nd). These correlations, excluding the two dredge 52 samples (crosses), are all statistically significant, with $^{87}Sr/^{86}Sr$ and $^{143}Nd/^{144}Nd$ correlating significantly better with Sm/Nd than with Rb/Sr. Note that the two dredge 52 samples are far more depleted in Rb versus Sr than in Nd versus Sm (relative to their isotopic ratios) compared with other samples.

enrichment with respect to these elements (see below). Note that the lesser depletion of Nb relative to Rb and K in the N-MORB source cannot be explained by a differential enrichment but may be an intrinsic characteristic of the depleted mantle, which may partly complement the Nb depletion in the continental crust. Further study is, however, required to fully assess the global implications of this result.

E-MORB Mantle Source Heterogeneity Beneath the Hump Area and the Southern EPR

The southern seamount SE group samples are typical E-MORB having more radiogenic Sr and Pb and less radiogenic Nd than N-MORB and elevated abundances of incompatible elements. Even so, there is still an excess of highly incompatible elements (Figures 5, 8, and 9). The excess is even clearer in Figure 10 and represents an enrichment superimposed on a preexisting enriched character. Most E-MORB along the entire southern EPR (13° to 23°S) are characterized by an excess enrichment of highly incompatible elements yet have isotopic signatures similar to those of nearby N-MORB; that is, incompatible elements and isotopes are decoupled [*Mahoney et al.*, 1994]. For convenience, we call this type "decoupled" E-MORB and those showing correlations between incompatible element ratios and radiogenic isotopes "coupled" E-MORB, such as the Hump area SE group samples.

Coupled E-MORB. Basalts with elevated abundances of incompatible elements and "enriched" radiogenic isotopic characteristics, such as the Hump SE group samples (see Figures 5 and 7), are very common from both the axis and off-axis seamounts in the plume-absent northern EPR [e.g., *Batiza and Vanko*, 1984; *Zindler et al.*, 1984; *Graham et al.*, 1988; *Hékinian et al.*, 1989; *Castillo et al.*, 1991; *Niu et al.*, 1994], indicating the existence of enriched domains in the ambient depleted mantle, which may represent remnants of ancient subducted oceanic crust or detached continental lithosphere that survived in the convecting mantle (see *Zindler and Hart* [1986] and *Carlson* [1994] for reviews). Regardless of the ultimate source, the enriched domains beneath the Hump area in the southern EPR must have come from a less degassed region in the mantle as shown by plume-like high $^{3}He/^{4}He$ ratios in the axial lavas [*Mahoney et al.*, 1994]. *Mahoney et al.* [1994] speculated that the plume-like component may have originated via asthenospheric flow from a plume associated with either the Easter or Marquesas hotspot. Mantle tomography [*Phipps Morgan et al.*, 1995], indeed, suggests that such plume material may have been contaminating the east Pacific mantle for some time.

Table 5. Partition Coefficients Used in This Study

	Pl	Ol	Cpx	Opx	Sp	Gnt
Sc	0.0200	0.1700	3.0000	1.2000	0.0480	4.0000
Ti	0.0100	0.0160	0.3000	0.1000	0.1000	0.6000
V	0.0100	0.0900	1.5000	0.6000	38.0000	3.0000
Cr	0.0100	0.2000	10.0000	5.0000	10.0000	3.0000
Ni	0.0100	10.0000	2.0000	5.0000	5.0000	1.1000
Sr	2.0000	0.0160	0.2600	0.0160	0.0001	0.2000
Y	0.0700	0.0100	0.4850	0.0800	0.0078	2.7500
Zr	0.0100	0.0100	0.1000	0.0500	0.0500	0.5000
Nb	0.0090	0.0020	0.0050	0.0025	0.0004	0.0005
K	0.0168	0.0010	0.0053	0.0039	0.0003	0.0005
P	0.0250	0.0002	0.2563	0.0145	0.0005	0.0050
La	0.0400	0.0001	0.1000	0.0053	0.0003	0.0005
Ce	0.0350	0.0001	0.1625	0.0090	0.0005	0.0080
Pr	0.0300	0.0002	0.2250	0.0127	0.0007	0.0325
Nd	0.0250	0.0003	0.2875	0.0163	0.0008	0.0570
Sm	0.0200	0.0006	0.3500	0.0200	0.0009	0.2170
Eu	0.5000	0.0048	0.3800	0.0275	0.0009	0.4500
Gd	0.0150	0.0090	0.4100	0.0350	0.0011	0.9667
Tb	0.0130	0.0132	0.4400	0.0480	0.0013	1.4833
Dy	0.0110	0.0174	0.4700	0.0610	0.0015	2.0000
Ho	0.0090	0.0216	0.5000	0.0740	0.0023	2.7500
Er	0.0070	0.0258	0.4833	0.0870	0.0030	3.5000
Yb	0.0050	0.0300	0.4667	0.1000	0.0045	7.0000
Lu	0.0030	0.0342	0.4500	0.1130	0.0050	10.0000

Pl, plagioclase; Ol, olivine; Cpx, clinopyroxene; Opx, orthopyroxene; Sp, spinel; Gnt, garnet. Data sources are *Irving* [1978], *Henderson* [1982], *McKay* [1986], *Dunn* [1987], *Green et al.* [1989], *Blundy and Wood* [1991], *Gallahan and Nielson* [1992], *Forsythe et al.* [1994], and *Hart and Dunn* [1993]. For modeling calculations, bulk $D_{Sr} = (D_{Pr} + D_{Nd})/2$ values were used based on Y. Niu's unpublished Inductively-coupled plasma mass spectrometer (ICP-MS) data (1996) of northern EPR seamount glasses.

Figure 12 shows the data for the entire southern EPR between 13° and 23°S. Although scatter exists, the axial data between the 15.8° and 20.7°S offsets, i.e., the isotopic "dome" of *Mahoney et al.* [1994] (Figure 2), form a cluster lying on the trends defined by the Hump area samples. This may suggest that the incompatible element-isotope coupling in the Hump area exists over a greater region of the mantle. If the seamount data manifest a melting-induced mixing relationship between the depleted MORB mantle and the enriched, plume-like component, as we interpret, then the axial lavas reflect processes of effective melt homogenization prior to eruption (e.g., melt aggregation during melt transport and magma mixing in crustal magma chambers) beneath the rise axis (versus off-axis seamounts). Thus the axial isotopic "dome" should be associated genetically with the origin of the enriched material apparent in the Hump area SE group seamount lavas.

Decoupled E-MORB. Two types of decoupling exist in the southern EPR. One is the southward monotonic decrease in incompatible element ratios of N-MORB from 13° to 23°S, which forms the regional background and which does not correlate with the latitudinal isotopic systematics (Figure 2). The other is the E-MORB characterized by elevated incompatible element ratios (i.e., the "excess" of highly incompatible elements versus moderately incompatible ones; see Figure 2) that are distributed randomly above the background yet have isotopic signatures similar to spatially associated N-MORB. This is particularly obvious in regions unaffected by the plume-like material outside the isotopic "domes", i.e., north of 15.8°S and south of 20.7°S offsets (Figure 12). *Sinton et al.* [1991] and *Mahoney et al.* [1994] interpreted the E-MORB of this type to have resulted from depleted mantle source that underwent incompatible element enrichment recently enough so as not to produce significant changes in Nd, Pb, and Sr isotopic ratios. We believe low-degree (low F) melts generated from the N-MORB depleted mantle are largely responsible for the decoupled E-MORB. Globally, as the decoupling does not require foreign material (i.e., isotopically exotic to the depleted mantle), such enrichment need not be associated with any single event but may have occurred throughout much of geological history. However, the low-F melts causing such enrichment must be generated at depths (P and T conditions) where the low-melting-point components reach their solidus deeper than that of dry peridotites in the upwelling mantle. In this regard, the "age" of the low-degree-melt generation should be roughly inversely related to the plate spreading rate. Assuming that (1) mantle upwelling rate is of the order of plate spreading rate (mean half-rate, ~ 80 mm/yr) and (2) the low-F melts form at a depth of ~ 250 km (the conservative deeper limit of the low-velocity zone), then the enrichment may be no older than 4 Myr beneath the superfast southern EPR.

Lavas having limited isotopic variations but variable incompatible element abundances and ratios have been previously observed [*Clague et al.*, 1981; *Perfit et al.*, 1983; *Hékinian and Walker*, 1987; *Frey et al.*, 1993]. Earlier efforts indicated that the enrichment of very incompatible elements is more than can be accounted for by simple crystallization, which became one of the persistent enigmas of MORB petrogenesis [e.g., *Perfit et al.*, 1983; *Sinton and Detrick*, 1992]. *Hékinian and Walker* [1987] interpreted this overenrichment to result from boundary layer crystallization or in situ fractionation [e.g., *Langmuir*, 1989]. *Frey et al.* [1993] showed that crustal-level fractionation is insufficient. *O'Hara* [1985] quantitatively showed that the extent of incompatible element enrichment may be controlled by the shape of the melting region. This effect is certainly functional in theory, but it cannot explain the occurrence of E-MORB which often coexists spatially with N-MORB along the EPR. *Plank and Langmuir* [1992] argued that the shape of the melting region is irrelevant and proposed that E-MORB represents mixtures of N-MORB magmas with very low F melts produced at the far corners of a hypothetical triangular melting region beneath the ridge. *Frey et al.* [1993] concluded that this type of E-MORB represents mixtures of melts derived from different extents of melting but argued that migration of very low F melts to the ridge axis envisioned by *Plank and Langmuir* [1992] is unrealistic.

We propose that such "mixing" is not simply a mixing of melts but instead takes place in the source region prior to major melting; that is, the source has been refertilized/infiltrated in the form of fine veins or dikes by the low-F melts generated from the depleted mantle. The evidence comes from the peculiar dredge 52 samples from a small southern seamount (see below). Small dikes or veins enriched in incompatible elements have been observed by submersible studies to be pervasive [*Cannat et al.*, 1990, 1992; *Hékinian et al.*, 1992, 1993, 1995] in the uppermost mantle, and some are extremely enriched (with apatite, zircon, etc.) [*Cannat et al.*, 1992]. The low-F melts should be enriched in very incompatible elements but may or may not be distinct in terms of radiogenic isotopes, depending on the source character of the low-F melts. For example, if the

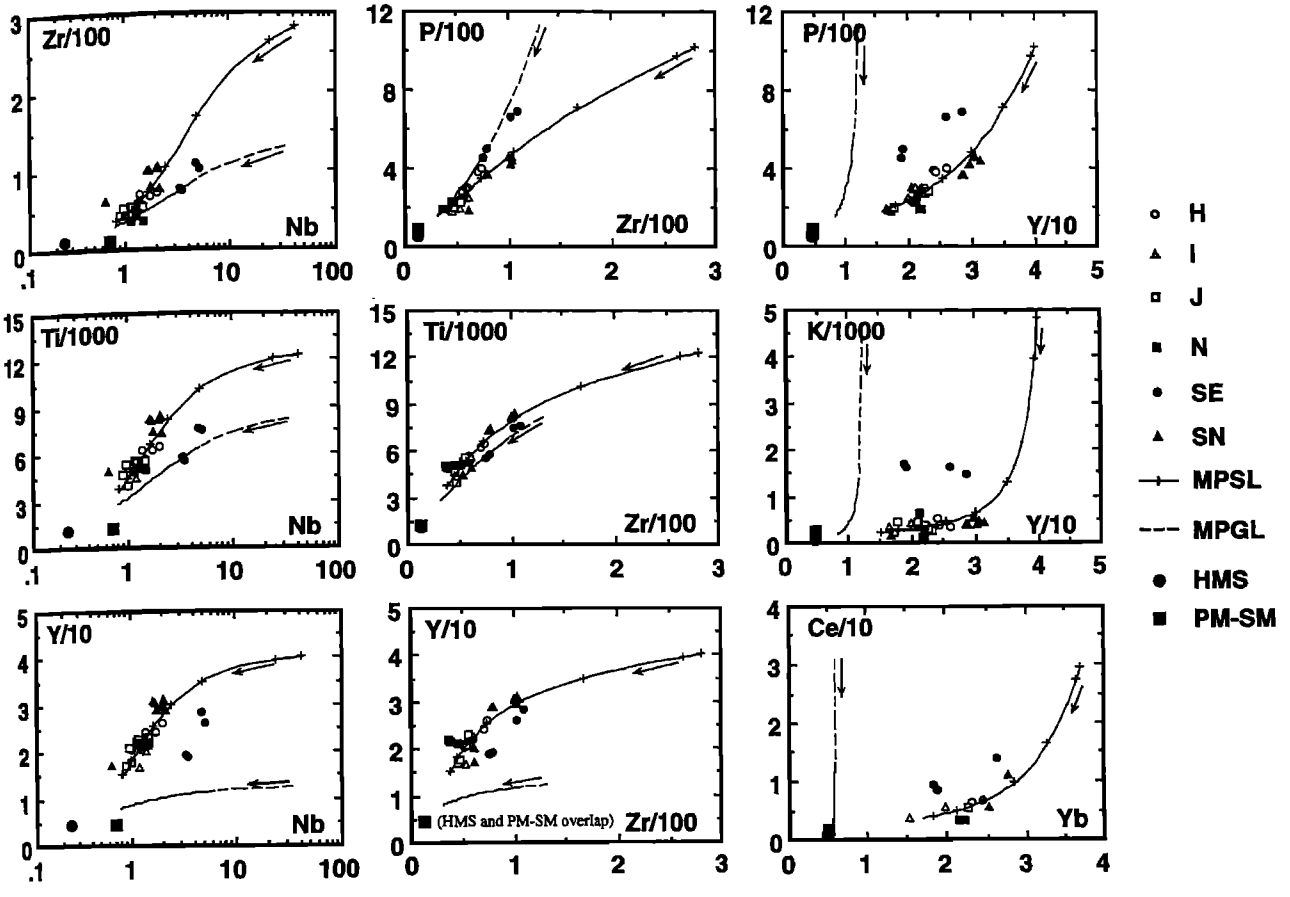

Figure 8. Element-element variation diagrams of the calculated primary Hump magmas together with calculated melting paths. Solid lines (arrows pointing to increasing melting) with ticks (0.5%, 1%, 2%, 5%, 10%, 15%, 20%, and 25%) represent melting in the spinel lherzolite field, and the dashed lines represent melting in the garnet lherzolite field (ranging from 0.5 to 20% melting with garnet being eliminated at 20.2% melting). HMS is our model mantle source, and PM-SM is the primitive mantle of *Sun and McDonough* [1989] for reference. The melting paths were calculated using the nonmodal batch and fractional melting models of *Shaw* [1970] for garnet and spinel lherzolite sources, respectively. Modal data are from *Johnson et al.* [1990]. See text for discussion.

low-F melts originate in the depleted mantle, then they remain isotopically identical to N-MORB, which explains the incompatible element-isotope decoupling in the southern EPR (Figures 2 and 11). If these low-F melt veins/dikes invade sites containing already enriched mantle, then this will result in an excess enrichment (e.g., the SE group lavas in the Hump area); if the mantle from which the low-F melts are derived differs isotopically from the ambient MORB mantle, then the low-F melts will also inherit a distinct isotopic signature. Our global data survey shows that depleted MORB mantle exhibits a large range of incompatible element ratios, even when isotopic ratios are similar, implying that low-F "metasomatic" melts derived from an isotopically "depleted" MORB source may be more important on a global scale than those from sources with a long-term history of enrichment in Rb, U, Th, and Nd.

Dredge 52: A puzzle and a solution. The two dredge 52 samples have about the highest $^{206}Pb/^{204}Pb$ and $^{87}Sr/^{86}Sr$ and lowest $^{143}Nd/^{144}Nd$ in the entire southern EPR region yet are highly depleted in incompatible elements (see Figures 2, 6, 7, and 12). These combined features can readily be reconciled with the low-F melt process discussed above. If parts of the mantle are enriched in incompatible elements by low-F-melt fertilization, then these elements must be correspondingly depleted in other parts of the mantle from which the low-F melts originate. It is clear from Figure 7 that these samples are more depleted in highly incompatible elements than in less incompatible ones (e.g., very low Rb/Sr versus moderate Sm/Nd) in comparison with other samples, an indication that the source of these lavas lost a substantial fraction of its incompatible elements by removal of a low-F melt component. Thus, in the southern seamounts, we see both effects of the low-F-melt process: local enrichment (melt destinations) and local depletion (melt origins). Note that lavas derived from a region of depleted mantle that had experienced recent low-F melt removal would be more difficult to recognize because they would not be isotopically distinctive.

Summary of the Origin of Mantle Source Heterogeneity Beneath the Hump Area and the Southern EPR

The data and foregoing discussion show that the mantle source heterogeneity is complex beneath the Hump area. The complexity is, however, readily explained by two independent

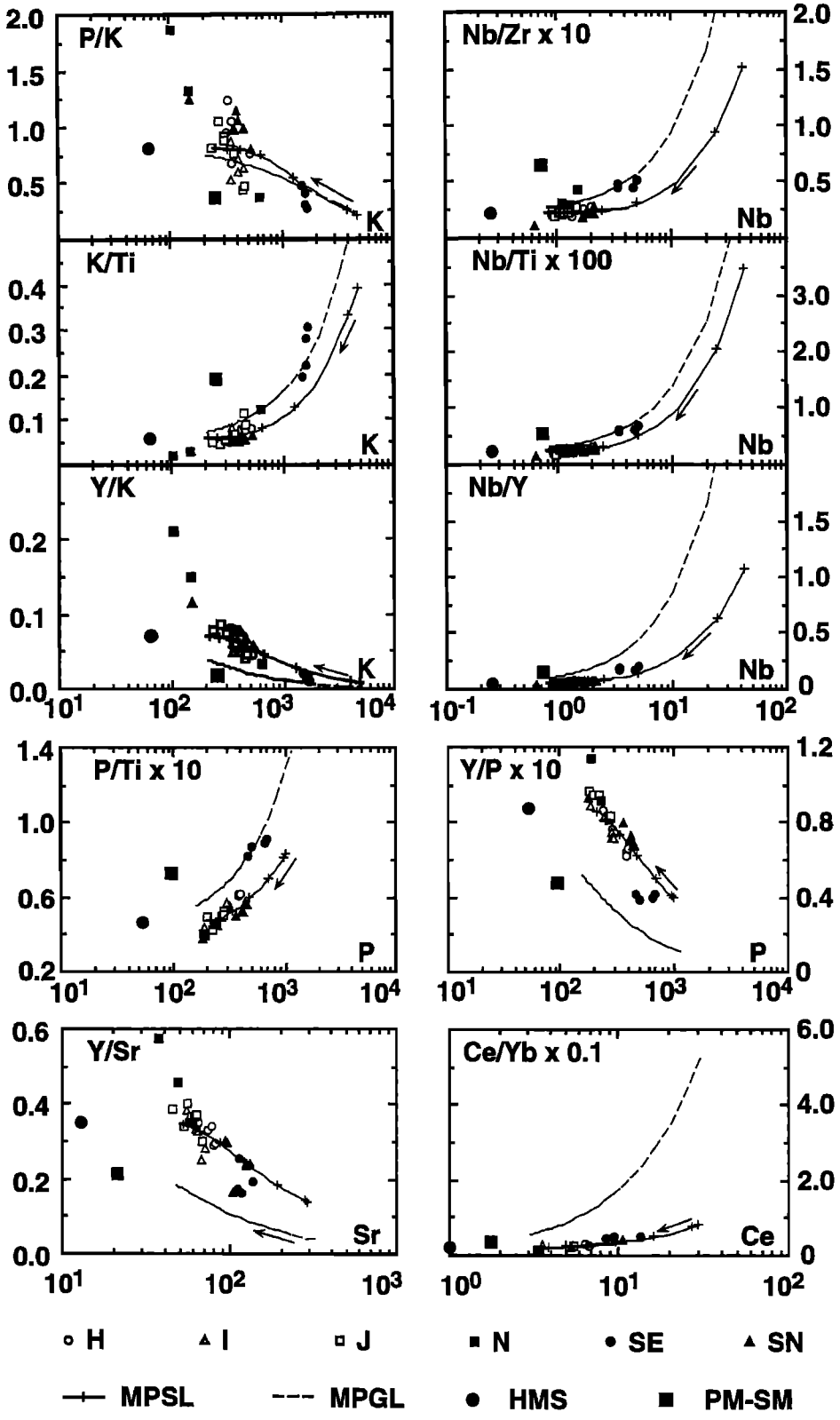

Figure 9. Ratio-element plots for calculated primary Hump magmas showing that the elemental relationships are more complicated than could be concluded from Figure 8. In general, the data are more scattered. The northern seamount lavas (N, small solid squares) are more depleted than could be achieved by > 25% melting on some diagrams, but not on others. The SE group samples exhibit enrichment in incompatible elements and are more enriched in highly incompatible elements than in less incompatible ones. The Ce/Yb-Ce panel shows that the trend defined by the data falls along the spinel (versus garnet) lherzolite melting path.

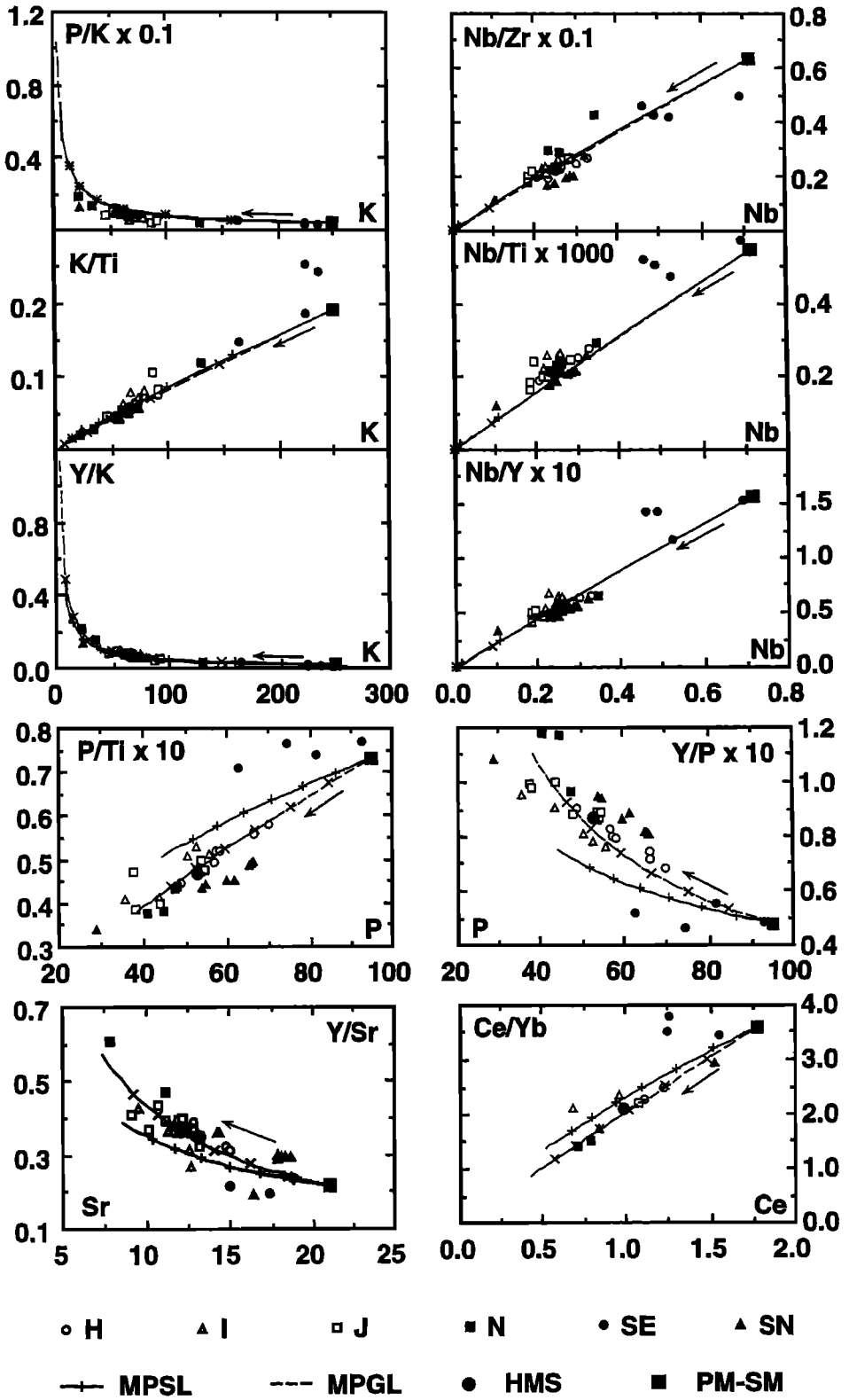

Figure 10. Same set of plots as in Figure 9 for the inferred mantle-source compositions for the Hump area lavas. The curves with symbols are depletion paths calculated for spinel lherzolite (solid line with pluses) and garnet lherzolite (dashed line with crosses) by melting the PM-SM. The tick marks represent the effects of 0.5%, 1%, 1.5%, 2%, 2.5%, and 3% melt removal. The HMS is also plotted for reference. Except for the SE sources, the calculated sources for the EPR axis and seamounts could represent 1-3% previous melt depletion from the PM. The plots of P/Ti-P, Y/P-P, Y/Sr-Sr, and Ce/Yb-Ce suggest that this melt depletion may have occurred at garnet lherzolite depths. SE sources, however, indicate an enrichment in all these elements, with a greater enrichment in more incompatible elements.

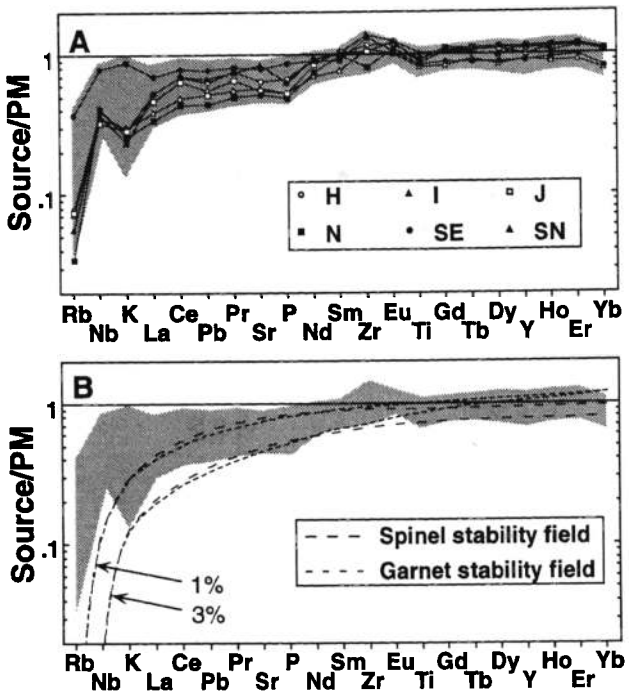

Figure 11. Primitive-mantle [*Sun and McDonough*, 1989]-normalized incompatible element patterns for the calculated Hump area sources. The shaded areas are the actual range. The lines with symbols in Figure 11a are the averages of individual ridge segments and grouped seamount types (as in Figures 8-10). The long and short dashed lines in Figure 11b approximate depletion from PM-SM as a result of 1% and 3% melting in both the spinel and garnet stability fields, which explain the overall patterns of the estimated Hump area mantle sources. Note that such a depletion cannot explain the less depleted nature of highly incompatible elements (e.g., Rb, Nb, and K). Also note that Nb is less depleted than Rb and K.

processes: process 1, invasion of plume-like material in the ambient depleted mantle, and process 2, the emplacement of enriched veins or dikes in the depleted mantle in the recent past by low-F melts derived primarily from the same depleted mantle.

Process 1 explains the significant correlations between radiogenic isotope ratios and ratios of incompatible elements for the entire Hump area (excluding the dredge 52 samples and the overabundance of highly incompatible elements in the SE group lavas). These correlations are binary mixing relationships resulting from melting of a source that is compositionally heterogeneous, with the two end-members having distinct trace element and isotopic signatures. The enriched material has a weakly plume-like character and occurs as domains of variable sizes distributed irregularly in the ambient depleted mantle prior to major melting events. The axial lavas that define the isotopic "dome" between 15.8° and 20.7°S can be explained likewise. The ultimate origin of the enriched material is yet to be understood, but it must be ancient and must come from a less degassed region in the mantle. As suggested by *Mahoney et al.* [1994], the enriched plume-like material may come from the French Polynesian hotspots as a result of eastward asthenospheric flow [*Phipps Morgan et al.*, 1995].

Process 2 explains the obvious decoupling between incompatible (especially highly incompatible) elements and isotopes throughout the entire southern EPR (13° to 23°S) and the overenrichment of highly incompatible elements of the Hump SE group lavas. Infiltration of low-F melts derived from the same depleted mantle at depth (prior to a major melting events) is perhaps an important process throughout the depleted mantle. The consequence of such a process is to produce localized enriched heterogeneities as fine veins or dikes with essentially the same isotopic characteristics: melting of such a source will inevitably result in melts with incompatible element-isotope decoupling. The dredge 52 samples reflect the existence of an isotopically distinct mantle "domain", but it represents a site of the low-F melt generation.

Seamount Formation, Mantle Melting Beneath the EPR, and Tectonics

Batiza et al. [1990] showed that near-ridge seamount volcanism is an integral part of the mantle melting system beneath the EPR, which favors a broad zone of mantle upwelling [e.g., *Reid and Jackson*, 1981; *Phipps Morgan*, 1987]. By assuming $F_{MEAN} \approx 10\%$, a broad (~ 120 km) zone of upwelling and melting, with complete melt extraction, is apparently needed to produce the observed crustal thickness at the very narrow (1 - 2 km) neovolcanic zone [e.g., *Phipps Morgan*, 1987]. Consequently, great efforts have been expended to elaborate mechanisms on how melts focus toward the axis over long distances (> 60 km) of melt migration (see reviews by *Turcotte and Phipps Morgan* [1992]). Recently, *Cordery and Phipps Morgan* [1993] demonstrated this process to be impossible without invoking boundary layer channeling beneath the cold lithosphere lid [*Sparks and Parmentier*, 1991]. We believe that such long-distance (> 60 km) melt migration does not occur because (1) geochemical data of near-ridge seamounts provide no evidence, (2) the value of $F_{MEAN} = 10\%$, which is used to constrain melt production, is erroneously low, and (3) most of the melt forms in the center of the upwelling zone even though the melting zone is wide as a result of enhanced upwelling rate beneath the axis where a component of buoyant upwelling exists [e.g., *Scott and Stevenson*, 1989; *Buck and Su*, 1989; *Niu and Batiza*, 1991b] (Figures 13a and 13b).

The differential mantle upwelling across the ridge axis will also promote development of vertical/subvertical shear planes, which will facilitate melt migration and focusing toward the ridge axis (Figure 13b). Away from the axis, the shear planes gradually bend over, inhibiting melt focusing toward the axis but making seamount volcanism possible if zones of weakness exist in the lithosphere [e.g., *Sleep*, 1988]. Evidence of shear-facilitated melt transport is widely observed in ultramafic sections of many ophiolite suites [e.g., *Nicolas*, 1989; *Ceuleneer and Rabinowicz*, 1992; *Kelemen and Dick*, 1995]. Collectively, all the observations indicate that seamount volcanism and axial volcanism share a common thermal environment, encompassing a broad zone of mantle upwelling and melting [*Batiza et al.*, 1990; *Niu and Batiza*, 1991a], yet melt production rate is the highest beneath the axis and decreases with distance away from the axis [*Niu and Batiza*, 1991a]. In such an environment, seamount and axial volcanism should have different supply mechanisms: shear-induced vertical/subvertical melt migration and focusing for axial eruptions and tectonics/structure-controlled magma pumping ("leaks") at off-axis seamounts (Figure 13b).

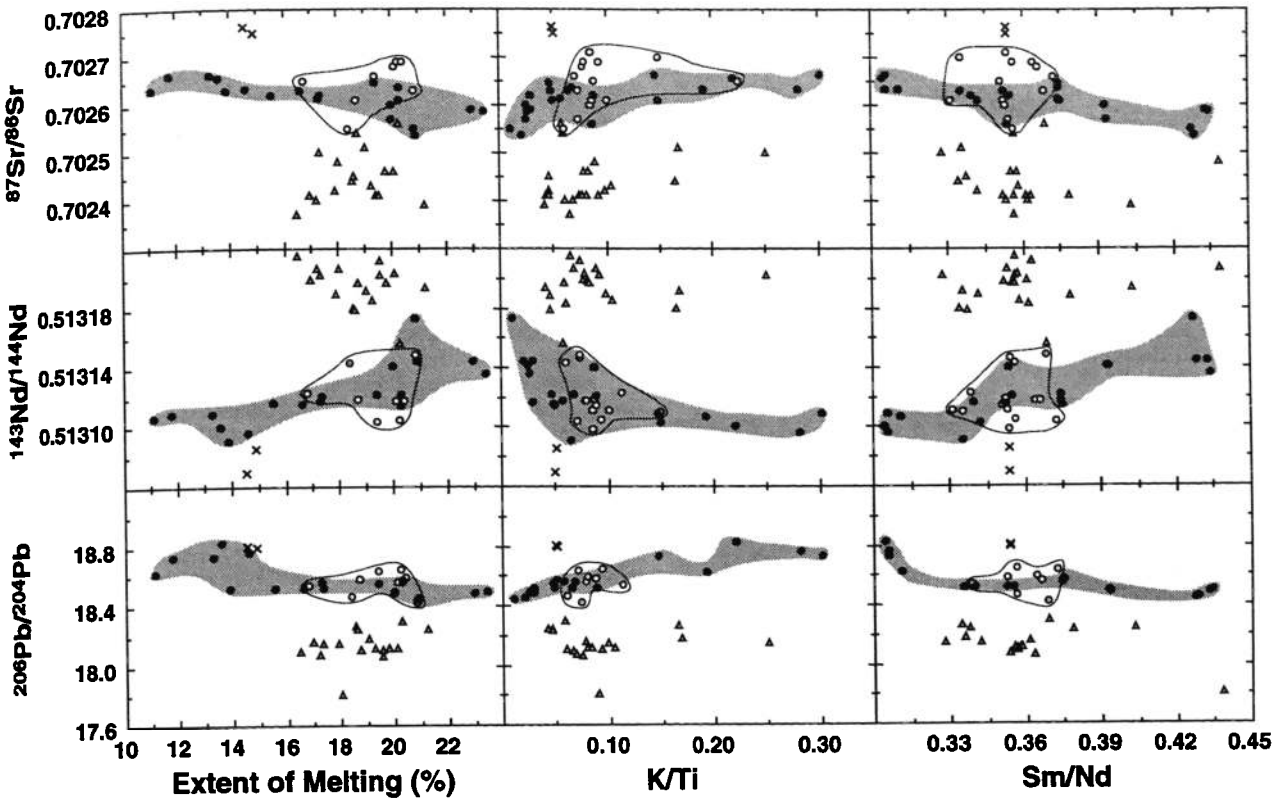

Figure 12. Similar to Figures 6 and 7 but includes all the data of *Mahoney et al.* [1994] for the entire southern EPR (13° to 23°S). Solid circles are for the Hump lavas (both axis and seamounts), open circles are for axial lavas between 15.8°S and 20.7°S offsets (i.e., the isotopic dome in Figure 2), open triangles are lavas from north of the 15.8°S and south of the 20.7°S offsets, and crosses are for dredge 52 samples. Note that although more scattered in Nd and Sr isotope values with respect to relatively restricted range of K/Ti, Sm/Nd, and the extent of melting, the axial data in the 15.8° - 20.7°S region form a cluster lying on the trends defined by the Hump seamount lavas. Also note that lavas north of the 15.8°S and south of the 20.7°S offsets are isotopically "depleted", yet exhibit a large range of incompatible element ratios.

Seamounts may be initiated very near the ridge axis as a result of variations in melting geometry caused by ridge segmentation and associated structural weaknesses [e.g., *Lonsdale*, 1985; *Batiza*, 1989, 1991]. Seamount growth can be maintained by continuous or episodic melt discharge through preexisting feeders until the feeder systems are eradicated by horizontal shearing as the plate moves away from the axis (Figure 13b), which explains why near-ridge seamount chains are short, < 100 km (versus hotspot tracks). Existing models concerning seamount formation include deep-rooted, fixed, melting anomalies [*Davis and Karsten*, 1986] or minihotspots (or miniplumes) [e.g., *Shen et al.*, 1993, 1995], ridge-perpendicular convection rolls [e.g., *Buck and Parmentier*, 1986], and by-products of narrow, dynamic upwelling [*Wilson*, 1992]. These models, however, cannot explain (1) extremely depleted geochemical signatures in many seamount lavas and (2) how "miniplumes" could survive penetrating through the uppermost asthenosphere which is partially molten near the ridge axis.

Summary and Conclusions

1. The chemical diversity of the Hump area lavas can be explained if crustal-level fractionation, extent of partial melting, and mantle source heterogeneity are all considered.

2. Lava major element chemistry preserves the information on melting conditions, whereas incompatible-trace-element data reflect the previous history of the mantle source material. Caution is necessary when using trace element data alone to model melting processes.

3. The calculated mean extent of melting for the Hump area ranges from ~ 14% for the southern seamount group to ~ 22% for the northern seamount group, with axial lavas representing 18% to 19% melting, consistent with Ti-Na melting relationships and the observations that mantle melting residues beneath the EPR are highly depleted harzburgite.

4. The E-type MORB source heterogeneity is complex but is readily explained by two independent processes. (1) Invasion of plume-like material (possibly from French Polynesian hotspots to the west) into the ambient depleted mantle explains the significant correlations among isotopic ratios, ratios of incompatible elements, and the extent of melting derived from major elements. These correlations are binary mixing relationships resulting from melting of a heterogeneous mantle containing irregularly distributed, enriched (plume-like) domains of variable sizes. Axial lavas that form the isotopic "dome" between 15.8° and 20.7°S can be explained likewise. (2) Infiltration in the source region by low-degree melts derived primarily from depleted mantle in the recent past explains the excesses of highly incompatible

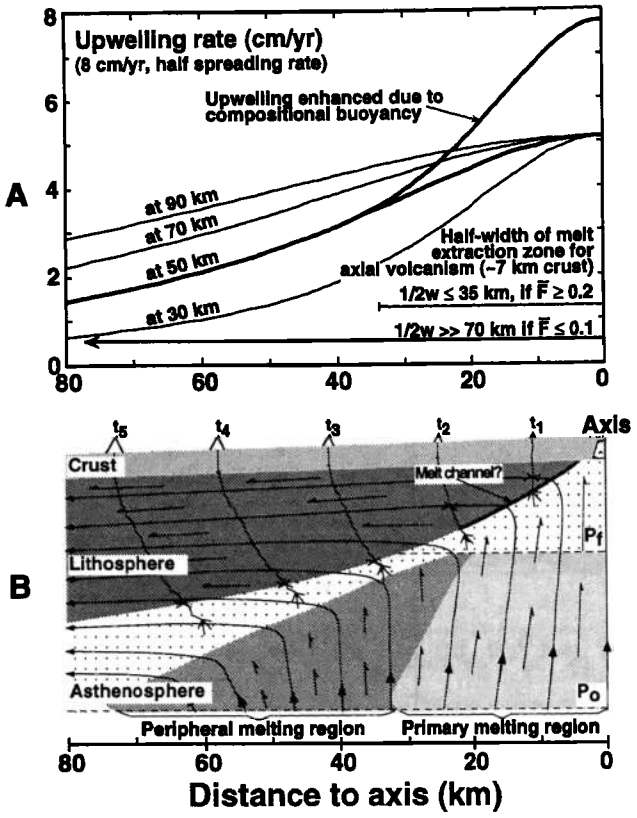

Figure 13. (a) Mantle upwelling rate varies with both depth (e.g., at 90, 70, 50, and 30 km) and distance to ridge axis beneath a ridge for a perfectly passive upwelling [e.g., *Turcotte and Phipps Morgan*, 1992]. The upwelling rate is enhanced in the center of the region when compositional buoyancy due to melt depletion is considered (e.g., assuming a mean melt extraction depth of 50 km). Thus most melt is generated in the central region beneath the axis. If $F_{MEAN} \geq 20\%$, melt extracted from this central region (< 35 km on both sides of the axis) will be sufficient for the ~ 7-km crust. (b) Near-ridge seamount volcanism is an integral part of the melting system beneath the EPR. The important elements are (1) mantle flow lines (solid lines with full double-headed arrows); (2) initial, Po, and final, Pf, depths of melting; (3) regions of primary and peripheral melting; (4) seamounts, seamount initiation, and growth; and (5) shear planes due to differential upwelling (line segments with single-headed arrows). Extraction of melt formed in the primary melting region leads to crust formation at the axis, with melt migration/focusing facilitated by vertical/subvertical shear planes and also perhaps by a melt channel beneath the young lithosphere near the axis. Seamounts may initiate near the axis (e.g., t_1 and t_2) and grow by continuous/episodic melt discharge through existing feeders until the feeder systems are eradicated by horizontal shearing. Melts formed in the peripheral melting region may never contribute to axial volcanism but are available for seamount volcanism. Note that melt migration/focusing beneath ridge axis is an important melt aggregation (mixing) process. In contrast, seamounts may only drain "free" melts locally formed in the peripheral melting region.

elements in the Hump area E-MORB and the incompatible element-isotope decoupling throughout the southern EPR (13° to 23°S) axis. This process is, perhaps, more important on a global scale than a long-term history of enrichment in Rb, U, Th, and Nd in creating heterogeneities in the depleted MORB mantle.

5. The N-MORB source variation is consistent with 1-3% previous melt depletion in the garnet stability depth range from a primitive mantle. A lesser depletion of Nb relative to Rb and K may be an intrinsic characteristic of the depleted mantle and may partly complement the Nb depletion in the continental crust.

6. We confirm that near-ridge seamount volcanism is an integral part of the melting system beneath the EPR. However, axial and seamount lavas have different melt-supply mechanisms: shear-induced vertical/subvertical melt migration and focusing for axial eruptions and tectonics/structure controlled magma pumping ("leaks") at off-axis seamounts.

Acknowledgments. Cruise MW8712 and analytical work at SOEST were supported by NSF grants OCE-86-0880 and OCE-89-22978 to JMS and JJM. We thank R. Batiza and A. Ewart for helpful discussions. JMS thanks P. Robinson for help with the REE analyses at the University of Tasmania. Reviews by M. Flower, P. Michael, and W. Melson improved the paper significantly. This is SOEST contribution 4088.

References

Aggrey, K. E. D., D. W. Muenow, and R. Batiza, Volatile abundances in basaltic glasses from seamounts flanking the East Pacific Rise at 21°-14°N, *Geochim. Cosmochim. Acta*, *52*, 2115-2119, 1988.

Allègre, C. J., B. Hamelin, and B. Dupré, Statistical analyses of isotopic ratios in MORB: The mantle blob cluster model and the convective regime of the mantle, *Earth Planet. Sci. Lett.*, *71*, 71-84, 1984.

Auzende, J.-M., J. M. Sinton, V. Ballu, R. Batiza, D. Bideau, M.-H. Cormier, Y. Fouquet, P. Geistdofer, Y. Lagabrielle, and P. Spadea, Submersible observations at superfast spreading: NAUDUR program, East Pacific Rise, 17 - 19 degrees south (abstract), *Eos Trans. AGU*, *75* (16), Spring Meet. Suppl., 329, 1994.

Bach, W., E. Hegner, E. Erzinger, and M. Satir, Chemical and isotopic variations along the superfast spreading East Pacific Rise from 6° to 30°S, *Contrib. Mineral. Petrol.*, *116*, 365-380, 1994.

Bäcker, H., J. Lange, and V. Marchig, Hydrothermal activity and sulfide formation in axial valleys of the East Pacific Rise crest between 18 and 22°S, *Earth Planet. Sci. Lett.*, *72*, 9-22, 1985.

Baker, M. B., and E. M. Stolper, Determining the composition of high-pressure mantle melts using diamond aggregates, *Geochim. Cosmochim. Acta*, *58*, 2811-2827, 1994.

Batiza, R., Seamounts and seamount chains, in *The Geology of North America*, vol. N, *The Eastern Pacific Ocean and Hawaii*, edited by E. L. Hussong and D. M. Baker, pp. 289-306, Geol. Soc. of Am., Boulder, Colo., 1989.

Batiza, R., The Pacific Ocean crust, in *Oceanic Basalts*, edited by P. A Floyd, pp. 246-288, Blackie, Glasgow, 1991.

Batiza, R., and Y. Niu, Petrology and magma chamber processes at the East Pacific Rise ~ 9°30'N, *J. Geophys. Res.*, *97*, 6779-6797, 1992.

Batiza, R, and D. A. Vanko, Petrology of young Pacific seamounts, *J. Geophys. Res*, *89*, 11,235–11,260, 1984.

Batiza, R., B. R. Rosendahl, and R. L. Fisher, Evolution of oceanic crust. 3, Petrology and chemistry of basalts from the East Pacific Rise and Siqueiros transform fault, *J. Geophys. Res*, *82*, 265–276, 1977.

Batiza, R., T. L. Smith, and Y. Niu, Geologic and Petrologic evolution of seamounts near the EPR based on submersible and camera study, *Mar Geophys. Res.*, *11*, 169–236, 1989.

Batiza, R., Y. Niu, and W. C. Zayac, Chemistry of seamounts near the East-Pacific Rise: Implications for the geometry of sub-axial mantle flow, *Geology*, *18*, 1122-1125, 1990.

Blundy, J. D., and B. J. Wood, Crystal-chemical controls on the partitioning of Sr and Ba between plagioclase feldspar, silicate melts, and hydrothermal solutions, *Geochim. Cosmochim. Acta*, *55*, 193-209, 1991.

Bougault, H., L. Dmitriev, J.- G. Schilling, A. Sobolev, J. L. Jordan, and H. D. Needham, Mantle heterogeneity from trace elements: MAR triple junction near 14°N, *Earth Planet. Sci. Lett.*, *88*, 27–36, 1988.

Buck, W. R., and E. M. Parmentier, Convection beneath young oceanic lithosphere: Implication for thermal structure and gravity, *J. Geophys. Res*, *91*, 1961–1974, 1986.

Buck, W. R. and W. Su, Focussed mantle upwelling below mid-ocean ridges due to feedback between viscosity and melting, *Geophys. Res. Lett.*, *16*, 641-644, 1989.

Basaltic Volcanism Study Project (BVSP), *Basalt Volcanism on the Terrestrial Planets*, 1286 pp., Pergamon, Tarrytown, N.Y., 1981.

Cannat, M., D. Bideau, and R. Hébert, Plastic deformation and magmatic impregnation in serpentinized ultramafic rocks from the Garrett transform fault (East Pacific Rise), *Earth Planet. Sci. Lett.*, *101*, 216-232, 1990.

Cannat, M., D. Bideau, and H. Bougault, Serpentinized peridotites and gabbros in the Mid-Atlantic Ridge axial valley at 15°37'N and 16°52'N, *Earth Planet. Sci. Lett.*, *109*, 87-106, 1992.

Carlson, R. W., Mechanisms of earth differentiation: Consequences for the chemical structure of the mantle, *Rev. Geophys.*, *32*, 337-363, 1994.

Castillo, P. R., W. White, K. Harpp, R. Batiza, and Y. Niu, Petrology and Sr, Nd, and Pb isotope geochemistry of MORB from the 14° to 15°N segment of EPR (abstract). *Eos Trans. AGU*, *72*(44), Fall Meet. Suppl., 525, 1991.

Ceuleneer, G., and M. Rabinowicz, Mantle flow and melt migration beneath oceanic ridges: Models derived from observations in ophiolites, in *Mantle Flow and Melt Generation at Mid-Ocean Ridges*, *Geophys. Monogr. Ser.*, vol. 7, edited by J. P. Morgan, D. K. Blackman, and J. M. Sinton, pp. 123-154, AGU, Washington, D. C., 1992.

Clague, D. A., F. A. Frey, G. Thompson, and S. Rindge, Minor and trace element geochemistry of volcanic rocks dredged from the Galapagos spreading center: Role of crystal fractionation and mantle heterogeneity, *J. Geophys. Res.*, *86*, 9469-9482, 1981.

Cordery, M. J., and J. Phipps Morgan, Convection and melting at Mid-Ocean ridges, *J. Geophys. Res.*, *98*, 19,477-19,503, 1993.

Cormier, M.-H., and K. C. Macdonald, East Pacific Rise 18°-19°S: Asymmetric spreading and ridge reorientation by ultrafast migration of axil discontinuities, *J. Geophys. Res.*, *99*, 543-564, 1994.

Davis, E. E., and J. L. Karsten, On the cause of the asymmetric distribution of the seamounts about the Juan de Fuca ridge: Ridge crest migration over heterogeneous asthenosphere, *Earth Planet. Sci. Lett.*, *79*, 385-396, 1986.

Detrick, R. S., A. J. Harding, G. M. Kent, J. A. Orcutt, J. C. Mutter, and P. Buhl, Seismic structure of the southern East Pacific Rise, *Science*, *259*, 499-504, 1993.

Dunn, T., Partitioning of Hf, Lu, Ti, and Mn between olivine, clinopyroxene and basaltic liquid, *Contrib. Mineral. Petrol.*, *96*, 476-484, 1987.

Fitton, J. G., and D. James, Basic volcanism associated with intraplate linear features, *Philos. Trans. R. Soc. London Ser. A*, *317*, 253-266, 1986.

Forsyth, D. W., Crustal thickness and the average depth and degree of melting in fractional melting models of passive flow beneath mid-ocean ridges, *J. Geophys. Res.*, *98*, 16,073-16,079, 1993.

Forsythe, L. M., R. L. Nielson, and M. R. Fisk, High-field strength element partitioning between pyroxene and melt in basalts to dacites, *Chem. Geol.*, *117*, 107-126, 1994.

Frey, F. A., N. Walker, D. Stakes, S. R. Hart, and R. Nielson, Geochemical characteristics of basaltic glasses from the AMAR and FAMOUS axial valleys, Mid-Atlantic Ridge (36° - 37°N): Petrogenetic implications, *Earth Planet. Sci. Lett.*, *115*, 117-136, 1993.

Gallahan, W. E., and R. L. Nielson, The partitioning of Sc, Y, and the rare earth elements between high-Ca pyroxene and natural mafic to intermediate lavas at one atmosphere, *Geochim. Cosmochim. Acta*, *56*, 2387-2404, 1992.

Gillis, K., K. Mevel, and Scientific Party, *Proceedings of the Ocean Drilling Program, 147/148*, pp. 1-366, Ocean Drill. Program, College Station, Tex., 1993.

Graham, D. W., A. Zindler, M. D. Kurz, W. J. Jenkins, R. Batiza, and H. Staudigel, He, Pb, Sr, and Nd isotope constraints on magma genesis and mantle heterogeneity beneath young Pacific seamounts, *Contrib. Mineral. Petrol.*, *99*, 446-463, 1988.

Green, T. H., S. H. Sie, C. G. Ryan, and D. R. Cousens, Proton microprobe determined partitioning of Nb, Ta, Zr, Sr, and Y between garnet, clinopyroxene and basaltic magma at high pressure and temperature; *Chem. Geol.*, *74*, 201-216, 1989.

Hanson, G. N., Geochemical evolution of the suboceanic mantle, *J. Geol. Soc. London*, *134*, 235-253, 1977.

Hanson, G. N., and C. H. Langmuir, Modelling of major elements in mantle systems using trace element approaches, *Geochim. Cosmochim. Acta*, *42*, 725-741, 1978.

Hart, S. R., and T. Dunn, Experimental cpx/melt partitioning of 24 trace elements, *Contrib. Mineral. Petrol.*, *113*, 1-8, 1993.

Hart, S. R., and A. Zindler, In search of bulk Earth composition, *Chem. Geol.*, *57*, 247-267, 1986.

Hékinian, R., and D. Walker, Diversity and spatial zonation of volcanic rocks from the East Pacific Rise near 21°N, *Contrib. Mineral. Petrol.*, *96*, 265-280, 1987.

Hékinian, R., G. Thompson, and D. Bideau, Axial and off-axial heterogeneity of basaltic rocks from the East Pacific Rise at 12°35'N-12°51'N and 11°26'N-11°30'N, *J. Geophys. Res.*, *94*, 17,437-17,463, 1989.

Hékinian, R., D. Bideau, M. Cannat, J. Franchteau, and R. Hébert, Volcanic activity and crust-mantle exposure in the ultrafast Garrett transform fault near 13°28'S in the Pacific, *Earth Planet. Sci. Lett.*, *108*, 259-275, 1992.

Hékinian, R. D. Bideau, J. Franchteau, J. L. Cheminee, R. Armijo, P. Lonsdale, and N. Blum, Petrology of the East Pacific Rise crust and upper mantle exposed in Hess Deep (Eastern Equatorial Pacific), *J. Geophys. Res.*, *98*, 8069-8094, 1993.

Hékinian, R., D. Bideau, R. Herbért, and Y. Niu, Magmatic processes at upper mantle-crustal boundary zone: Garrett transform (EPR South), *J. Geophys. Res.*, *100*, 10,163-10,185, 1995.

Henderson, P., *Inorganic Geochemistry*, 353 pp., Pergamon, Tarrytown, N. Y., 1982.

Hirose, K., and I. Kushiro, Partial melting of dry peridotites at high pressures: Determination of compositions of melts segregated from peridotite using aggregates of diamond, *Earth Planet. Sci. Lett.*, *114*, 477-489, 1993.

Hofmann, A. W., Chemical differentiation of the Earth: The relationship between mantle, continental crust, and oceanic crust, *Earth Planet. Sci. Lett.*, *90*, 297-314, 1988.

Irving, A. J., A review of experimental studies of crystal/liquid trace element partitioning, *Geochim. Cosmochim. Acta*, *42*, 743-770, 1978

Johnson, K., H. B. Dick, and N. Shimizu, Melting in the oceanic upper mantle: An ion microprobe study of diopside in abyssal peridotites, *J. Geophys. Res.*, *95*, 2661–2678, 1990.

Kelemen, P. B., and H. J. B. Dick, Focused melt flow and localized deformation in the upper mantle: Juxtaposition of replacive dunite and ductile shear zones in the Josephine peridotite, SW Oregon, *J. Geophys. Res.*, *100*, 423-438, 1995.

Kingsley, R. H., and J.-G. Schilling, Carbon in Mid-Atlantic Ridge basaltic glasses from 28°N to 63°N: Evidence for a carbon-enriched Azores mantle plume, *Chem. Geol.*, *129*, 31-53, 1995.

Kinzler, R. J., and T. L. Grove, Primary magmas of mid-ocean ridges basalts, 2, Applications, *J. Geophys. Res.*, *97*, 6907-6926, 1992.

Kinzler, R. J., and T. L. Grove, Corrections and further discussion of the primary magmas of mid-ocean ridge basalts, 1 and 2, *J. Geophys. Res.*, *98*, 22,339-22,347, 1993.

Klein, E. M., and C. H. Langmuir, Global correlations of ocean ridge basalt chemistry with axial depth and crustal thickness, *J. Geophys. Res.*, *92*, 8089–8115, 1987.

Kushiro, I., Y. Syono, and S. Akimoto, Melting of a peridotite nodule at high pressures and high water pressures, *J. Geophys. Res.*, *73*, 6023-6029, 1968.

Langmuir, C. H., Geochemical consequence of in-situ crystallisation, *Nature*, *340*, 199–205, 1989.

Langmuir, C. H., J. F. Bender, A. E. Bence, G. N. Hanson, and S. R. Taylor, Petrogenesis of basalts from the FAMOUS area: Mid-Atlantic Ridge, *Earth Planet. Sci. Lett.*, *36*, 133-156, 1977.

Langmuir, C. H., J. F. Bender, and R. Batiza, Petrological and tectonic segmentation of the East Pacific Rise, 5o30'-14°30'N, *Nature*, *332*, 422-429, 1986.

Langmuir, C. H., E. M. Klein, and T. Plank, Petrological systematics of mid-ocean ridge basalts: Constraints on melt generation beneath ocean ridges, in *Mantle Flow and Melt Generation at Mid-Ocean Ridges*, *Geophys. Monogr. Ser.*, vol. 71, edited by J. P. Morgan, D. K. Blackman, and J. M. Sinton, pp. 183-280, AGU, Washington, D. C., 1992.

Lonsdale, P., Non-transform offsets of the Pacific-Cocos plate boundary and their traces on the rise flanks, *Geol. Soc. Am. Bull.*, *96*, 313–327, 1985.

Lonsdale, P., Segmentation of the Pacific-Nazca spreading center, 1°N to 20°S, *J. Geophys. Res.*, *94*, 12,197–12,226, 1989.

Macdougall, J. D., and G. W. Lugmair, Extreme isotopic homogeneity among basalts from the southern East Pacific Rise: Mantle or mixing effect?, *Nature*, *313*, 209-211, 1985.

Macdougall, J. D., and G. W. Lugmair, Sr and Nd isotopes in basalts from the East Pacific Rise: Significance for mantle heterogeneity, *Earth Planet. Sci. Lett.*, *77*, 273-289, 1986.

Mahoney, J. J., J. H. Natland, W. M. White, R. Poreda, S. H. Bloomer, R. L. Fisher, and A. N. Baxter, Isotopic and geochemical provinces of the western Indian Ocean spreading centres, *J. Geophys. Res.*, *94*, 4033–4052, 1989.

Mahoney, J. J., J. M. Sinton, D. M. Kurz, J. D. Macdougall, K. J. Spencer, and G. W. Lugmair, Isotope and trace element characteristics of a super-fast spreading ridge: East Pacific Rise, 13 - 23°S, *Earth Planet. Sci. Lett.*, *121*, 173-193, 1994.

McKay, G. A., Crystal/liquid partitioning in basaltic systems: Extreme fractionation of REE in olivine, *Geochim. Cosmochim. Acta*, *50*, 69-79, 1986.

McKenzie, D., and R. K. O'Nions, Partial melt distributions from inversion of rare earth element concentrations, *J. Petrol.*, *32*, 1021–1091, 1991.

Melson, W. G., T. L. Vallier, T. L. Wright, G. Byerly, and J. Nelen, Chemical diversity of abyssal volcanic glass erupted along Pacific, Atlantic and Indian Ocean floor spreading centers, in *The Geophysics of the Pacific Ocean and its Margin: A Volume in Honor of George P. Woollard, Geophys. Monogr. Ser.*, vol. 19, edited by George P. Woollard et al., pp. 351-368, AGU, Washington, D. C., 1976.

Michael, P. J., Regionally distinctive sources of depleted MORB: Evidence from trace elements and H_2O, *Earth Planet. Sci. Lett.*, *131*, 301-320, 1995.

Mysen, B. O., and A. L. Boettcher, Melting of a hydrous mantle, II, Geochemistry of crystals and liquids formed by anatexis of mantle peridotite at high pressures and high temperatures as a function of controlled activities of water, hydrogen, and carbon dioxide, *J. Petrol.*, *16*, 549-593, 1975.

Natland, J. H., Partial melting of a lithologically heterogeneous mantle: Inferences from crystallisation histories of magnesian abyssal tholeiites from the Siqueiros Fracture Zone, in *Magmatism in Ocean Basins*, edited by A. D. Saunders and M. J. Norry, *Geol. Soc. Spec. Publ. London*, *42*, 41–70, 1989.

Nicolas, A., Structures of ophiolite and dynamics of oceanic lithosphere, 368 pp., Kluwer Acad., Norwell, Mass., 1989.

Nielsen, R. L., D. M. Christie, and F. M. Sprtel, Anomalously low sodium MORB magmas: Evidence for depleted MORB or analytical artifact?, *Geochim. Cosmochim. Acta*, *59*, 5023-5026, 1995.

Niu, Y., Mid-ocean ridge magmatism: Style of mantle upwelling, partial melting, crustal level processes, and spreading rate dependence ææ A petrologic approach, Ph.D. thesis, 250 pp., Univ. of Hawaii, Honolulu, 1992.

Niu, Y., and R. Batiza, An empirical method for calculating melt compositions produced beneath mid-ocean ridges: Application for axis and off-axis (seamounts) melting. *J. Geophys. Res.*, *96*, 21,753-21,777, 1991a.

Niu, Y., and R. Batiza, In-situ densities of silicate melts and minerals as a function of temperature, pressure, and composition. *J. Geol.*, *99*, 767-775, 1991b.

Niu, Y., and R. Batiza, Magmatic processes at the Mid-Atlantic Ridge ~ 26° S, *J. Geophys. Res.*, *99*, 19,719-19,740, 1994.

Niu, Y., K. D. Collerson, and R. Batiza, Temporal variability of mantle source heterogeneity beneath the East Pacific Rise at 11°20'N over the Last 600 Ka, *Eos Trans. AGU*, *75*(44), Fall Meet. Suppl., 742, 1994.

O'Hara, M. J., The bearing of phase equilibria studies in synthetic and natural systems on the origin and evolution of basic and ultrabasic rocks, *Earth Sci. Rev.*, *4*, 69-133, 1968.

O'Hara, M. J., Importance of the "shape" of the melting regime during partial melting of the mantle, *Nature*, *314*, 58-62, 1985.

O'Nions, R. K., and D. P. McKenzie, Melting and continent generation, *Earth Planet. Sci. Lett.*, *90*, 449-456, 1988.

Perfit, M. R., D. J. Fornari, A. Malahoff, and R. W. Embley, Geochemical studies of abyssal lavas recovered by DSRV from Eastern Galapagos Rift, Inca Transform, and Ecuador Rift, 3, Trace element abundances and petrogenesis, *J. Geophys. Res.*, *88*, 10,551–10,572, 1983.

Perfit, M. R., D. J. Fornari, M. C. Smith, J. F. Bender, C. H. Langmuir, and R. M. Haymon, Small-scale spatial and temporal variations in mid-ocean ridge crest magmatic processes, *Geology*, *22*, 375-379, 1994.

Perram, L. J., H.-M. Cormier, and K. C. Macdonald, Magnetic and tectonic studies of the dueling propagating spreading centers at 20°40'S on the East Pacific Rise: Evidence for crustal rotations, *J. Geophys. Res.*, *98*, 13,835–13,850, 1993.

Phipps Morgan, J., Melt migration beneath mid-ocean ridge spreading centres, *Geophys. Res. Lett.*, *14*, 1238–1241, 1987.

Phipps Morgan, J., W. J. Morgan, Y.-S. Zhang, and W. H. F. Smith, Observational hints for a plume-fed, suboceanic asthenosphere and its role in mantle convection, *J. Geophys. Res.*, *100*, 12,753-12,767, 1995.

Plank, T., and C. H. Langmuir, Effects of the melting regime on the composition of the oceanic crust, *J. Geophys. Res.*, *97*, 19,749-19,770, 1992.

Prinzhofer, A., E. Lewin, and C. J. Allègre, Stochastic melting of the marble cake mantle: Evidence from local study of the East Pacific Rise at 12°50, *Earth Planet. Sci. Lett.*, *92*, 189-206, 1989.

Reid, I., and H. R. Jackson, Oceanic spreading rate and crustal thickness, *Mar. Geophys. Res.*, *5* , 165-172, 1981.

Renard, V., R. Hékinian, J. Franchteau, R. D. Ballard, and H. Bäcker, Submersible observations at the axis of the ultrafast-spreading East Pacific Rise (17°S to 21°30'S), *Earth Planet. Sci. Lett.*, *75*, 339–353, 1985.

Robinson, P., N. C. Higgins, and G. A. Jenner, Determination of rare earth elements, yttrium and scandium in rocks by an ion-exchange X-ray fluorescence technique, *Chem. Geol.*, *55*, 121-137, 1986.

Salters, V. J. M., and S. R. Hart, The hafnium paradox and the role of garnet in the source of mid-ocean ridge basalts, *Nature*, *342*, 420-422, 1989.

Saunders, A. D., M. J. Norry, and J. Tarney, Origin of MORB and chemically-depleted mantle reservoirs: Trace element constraints, *J. Petrol.*, *29*, 415-445, 1988

Scheirer, D. S., and K. C. Macdonald, Variation in cross-section area of the axial ridge along the East Pacific Rise: Evidence for the magmatic budget of a fast spreading center, *J. Geophys. Res.*, *98*, 7871-7885, 1993.

Schilling, J.- G., M. Zajac, R. Evans, T. Johnston, W. White, J. D. Devine, and R. Kingsley, Petrological and geochemical variations along the Mid-Atlantic Ridge from 29°N to 73°N, *Am. J. Sci.*, *283*, 510–586, 1983.

Scott, D. R., and D. J. Stevenson, A self-consistent model of melting, magma migration and buoyancy-driven circulation beneath Mid-Ocean Ridges, *J. Geophys. Res.*, *94*, 2973–2988, 1989.

Sempéré, J. -C., K. C. Macdonald, S. P. Miller, and L. Shure, Detailed study of the Brunshes/Matuyama reversal boundary on the East Pacific Rise at 19°30'S: Implications for crustal emplacement processes at an ultrafast spreading center, *Mar. Geophys. Res.*, *9*, 1-23, 1987.

Shaw, D. M., Trace element fractionation during anatexs, *Geochim. Cosmochim. Acta*, *34*, 237–243, 1970.

Shen, Y., and D. W. Forsyth, Geochemical constraints on initial and final depth of melting beneath mid-ocean ridges, *J. Geophys. Res.*, *100*, 2211-2237, 1995.

Shen, Y., D. W. Forsyth, D. S. Scheirer, and K. C. Macdonald, Two forms of volcanism: Implications for mantle flow and off-axis crustal production on the west flank of the southern East Pacific Rise, *J. Geophys. Res.*, *98*, 17,875 - 17,889, 1993.

Shen, Y., D. S. Scheirer, D. W. Forsyth, and K. C. Macdonald, Trade-off in production between adjacent seamount chains near the East Pacific Rise, *Nature*, *373*, 140-143, 1995.

Sinton, J. M., and R. S. Detrick, Mid-ocean ridge magma chambers, *J. Geophys. Res.*, *97*, 197–216, 1992.

Sinton, J. M., S. M. Smaglik, and J. J. Mahoney, Magmatic processes at superfast spreading mid-ocean ridges: Glass compositional variations along the East Pacific Rise 13°-23°S, *J. Geophys. Res.*, *96*, 6133-6155, 1991.

Sinton, J. M., L. S. Hall, J. Mahoney, R. Batiza, L. Norby, and M. Kurz, 3-D mantle heterogeneity and melting processes at superfast spreading: East Pacific Rise, 15-19 degrees south, *Eos Trans. AGU*, *75*(16), Spring Meet. Suppl., 330, 1994.

Sleep, N. H., Tapping of melts by veins and dykes, *J. Geophys. Res.*, *93*, 10,255–10,272, 1988.

Sparks, D. W., and E. M. Parmentier, Melt extraction from the mantle beneath spreading centres, *Earth Planet. Sci. Lett.*, *105*, 368–377, 1991.

Stolper, E., and S. Newman, The role of water in the petrogenesis of Mariana trough magmas, *Earth Planet. Sci. Lett.*, *121*, 293–325, 1994.

Sun, S.-S., and W. F. McDonough, Chemical and isotopic systematics of ocean basalt: Implications for mantle composition and processes, in *Magmatism of the Ocean Basins* edited by A. D. Saunders and M. J. Norry, *Geol. Soc. Spec. Publ. London*, *42*, 323-345, 1989.

Sun, S.-S., M. Tatsumoto, and J.-G. Schilling, Mantle plume mixing along the Reykjanes ridge axis: Lead isotope evidence, *Science*, *190*, 143-147, 1975.

Todt, W., R. A. Cliff, A. Hanser, and A. W. Hofmann, $^{202}Pb+^{205}Pb$ double spike for lead isotopic analysis, *Terra Cognita*, *4*, 209, 1984.

Turcotte, D. L., and J. Phipps Morgan, The physics of melt migration and mantle flow beneath a mid-ocean ridge, in *Mantle Flow and Melt*

Generation at Mid-Ocean Ridges, Geophys. Monogr. Ser., vol. 71, edited by J. P. Morgan, D. K. Blackman, and J. M. Sinton, pp. 155-182, AGU, Washington, D. C., 1992.

Walker, D., T. Shibata, and S. E. DeLong, Abyssal tholeiites from the Oceanographer Fracture Zone, II, Phase equilibria and mixing, *Contrib. Mineral. Petrol.*, *70*, 111-125, 1979.

Weaver, B. L., The origin of ocean island basalt end-member compositions: Trace element and isotopic constraints, *Earth Planet. Sci. Lett.*, *104*, 381-397, 1991.

Weaver, J. S., and C. H. Langmuir, Calculation of phase equilibrium in mineral-melt systems, *Comput. Geosci.*, *16*, 1–19, 1990.

Wilson, D. S., Focused mantle upwelling beneath mid-ocean ridges: Evidence from seamount formation and isostatic compensation of topography, *Earth Planet. Sci. Lett.*, *113*, 41-55, 1992.

Wood, D. A., A variably veined suboceanic upper mantle — Genetic significance for mid-ocean ridge basalts from geochemical evidence, *Geology*, *7*, 499-503, 1979.

Zindler, A., and S. R. Hart, Chemical geodynamics, *Annu. Rev. Earth Planet. Sci.*, *14*, 493–571, 1986.

Zindler, A., H. Staudigel, and R. Batiza, Isotope and trace element geochemistry of young Pacific seamounts: Implications for the scale of upper mantle heterogeneity, *Earth Planet. Sci. Lett.*, *70*, 175-195, 1984.

J. J. Mahoney, J. M. Sinton, and D. G. Waggoner, Department of Geology and Geophysics, University of Hawaii, Honolulu, HI 96822.

Y. Niu, Department of Earth Sciences, University of Queensland, Brisbane, Qld 4072, Australia. (e-mail: niu@earthsciences.uq.edu.au)

(Received November 29, 1995; revised June 3, 1996;
accepted June 7, 1996.)